

178
13

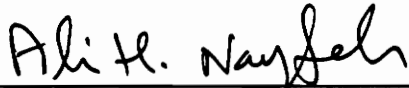
Nonlinear Dynamics in Power Systems

by

Mahir Ali Nayfeh

Thesis submitted to the Faculty of the
Virginia Polytechnic Institute and State University
in partial fulfillment of the requirements for the degree of
Master of Science
in
Electrical Engineering

APPROVED:



Dr. A. H. Nayfeh, Co-chairperson



Dr. W. T. Baumann, Co-chairperson



Dr. D. K. Lindner

May, 1990

Blacksburg, Virginia

c.2

LD
5655
V855
N395
1990
c.2

Nonlinear Dynamics in Power Systems

by

Mahir Ali Nayfeh

Dr. A. H. Nayfeh, Co-chairperson

Dr. W. T. Baumann, Co-chairperson

Electrical Engineering

(ABSTRACT)

We use a perturbation analysis to predict some of the instabilities in a single-machine quasi-infinite busbar system. The system's behavior is described by the so-called swing equation, which is a nonlinear second-order ordinary-differential equation with additive and multiplicative harmonic terms having the frequency Ω . When $\Omega \approx \omega_0$ and $\Omega \approx 2\omega_0$, where ω_0 is the linear natural frequency of the machine, we use digital-computer simulations to exhibit some of the complicated responses of the machine, including period-doubling bifurcations, chaotic motions, and unbounded motions (loss of synchronism). To predict the onset of these complicated behaviors, we use the method of multiple scales to develop approximate closed-form expressions for the periodic responses of the machine. Then, we use various techniques to determine the stability of the analytical solutions. The analytically predicted periodic solutions and conditions for their instability are in good agreement with the digital-computer results.

Acknowledgements

I wish to express my appreciation and gratitude to Professor Ali. H. Nayfeh, my advisor and father, for his support, guidance, and advice throughout my masters program. I like to thank Dr. Anan M. Hamdan for introducing me to the problem and for his valuable advice and guidance. I like to thank my committee members: Professor William T. Baumann and Professor Douglas K. Lindner for their comments and valuable advice. I thank Jamal Nayfeh, Bryan Heydon, Marwan Bikdash, and Balakumar Balachandran for their insightful discussions. I thank Michael Colbert for his valuable friendship, support, and advice throughout my undergraduate and graduate studies. Finally, a special thanks to Sally Shrader, her patience and expert typing skills were of great help.

Thanks are due to the Army Research Office for supporting this research under Grant No. DAAL03-89-K-0180.

I dedicate this work to my father and mother without their understanding, support, and encouragement this work would not have been done.

Table of Contents

Introduction	1
1.1 Formulation	6
1.2 Free Oscillation	8
Relevant Concepts of Nonlinear Dynamics	11
2.1 Equilibrium Points	13
2.1.1 Bifurcations of Equilibrium Points	14
2.2 Limit Cycles	16
2.2.1 Bifurcation of Limit Cycles	20
2.3 Torus or Quasi-periodic Attractors	21
2.4 Chaotic or Strange Attractor	21
2.4.1 Dimension	22
2.4.2 Liapunov Exponents and Dimension	23
2.4.3 Sensitivity to Initial Conditions	25
2.4.4 Power Spectrum	25
2.4.5 Transitions to Chaos	26
2.4.5.1 Torus Bifurcation Route to Chaos	26
2.4.5.2 Period-Doubling Route to Chaos	27

2.4.5.3 Intermittency	27
2.5 Invariant Manifolds	28
2.6 Poincaré Section	29
Primary Resonance	30
3.1 Introduction	30
3.2 Numerical Simulation	31
3.3 Perturbation Analysis	39
3.3.1 Comparison of the Perturbation Solution with Numerical Simulations	44
3.4 Stability of Period-One Solutions	47
3.4.1 Floquet Theory	47
3.4.2 Method of Strained Parameters	49
3.4.3 Harmonic Balance	53
3.4.4 Tangent Instability	54
Subharmonic Resonance	57
4.1 Introduction	57
4.2 Numerical Simulation	58
4.3 Perturbation Analysis	65
4.3.1 Comparison of the Perturbation Solution with Numerical Simulations	74
4.4 Stability of Periodic Solutions	77
Conclusions	79
5.1 Present Work	79
5.2 Future Work	81
References	82

Coefficients in Expanded Form of Swing Equation	89
Parameters of Machine Used in Chapter 3	90
Coefficients for Stability Analysis	91
Parameters of Machine Used in Chapter 4	92
Vita	93

List of Illustrations

Figure 1.	Single machine quasi-infinite busbar system	5
Figure 2.	Phase portrait of free oscillations	10
Figure 3.	Bifurcation patterns	17
Figure 4.	Numerical simulation for case of primary resonance	34
Figure 5.	Bifurcation diagram for case of primary resonance	36
Figure 6.	Basins of attraction ($\dot{\theta}$ vs. θ) for case of primary resonance	38
Figure 7.	Frequency-response curve for case of primary resonance	45
Figure 8.	Comparison of perturbation solution with numerical simulations for case of primary resonance	46
Figure 9.	Stability of perturbation solution for case of primary resonance	56
Figure 10.	Numerical simulation for case of subharmonic resonance	59
Figure 11.	Bifurcation diagram for case of subharmonic resonance	61
Figure 12.	Basins of attraction ($\dot{\theta}$ vs. θ) for case of subharmonic resonance	63
Figure 13.	Basins of attraction ($\dot{\theta}$ vs. θ) for case of subharmonic resonance	64
Figure 14.	Frequency-response curve for case of subharmonic resonance	75
Figure 15.	Comparison of perturbation and numerical solutions for case of subharmonic resonance	76
Figure 16.	Stability of perturbation solution for case of subharmonic resonance	78

CHAPTER 1

Introduction

The stability of a power system is closely related to the notion of a disturbance. A *disturbance* in a power system is a sudden change or a sequence of changes in one or more of the parameters of the system, or in one or more of the operating quantities (IEEE Task Force, 1982). A *small disturbance* is one for which the equations that describe the dynamics of the power system may be linearized for the purpose of analysis (IEEE Task Force, 1982). The tools of assessment for this type of stability belong to linear system theory, which includes eigenvalue analysis and frequency-response methods (Hughes and Hamdan, 1976; Hamdan, Hamdan, and Kahhaleh, 1989). A power system is *steady-state stable* for a particular steady-state operating condition if, following any small disturbance, it reaches a steady-state operating condition which is identical or close to the pre-disturbance operating condition; this is also known as *small disturbance stability*. A *large disturbance* is a disturbance

for which the equations that describe the dynamics of the power system cannot be linearized for the purpose of analysis (IEEE Task Force, 1982). The tools of assessment in this case belong to nonlinear dynamics, which includes numerical simulation as well as geometric methods and energy functions (Anderson and Fouad, 1977; Pai, 1981). The ability of the system to maintain synchronism under large disturbances is associated with transient stability (Pai, 1981). We are interested in disturbances that lead to a nonlinear representation; such a representation can be studied by using nonlinear-dynamic methods and perturbation techniques (Nayfeh, 1973,1981), which are widely used in nonlinear mechanics (Nayfeh and Mook, 1979). Perturbation techniques were used by Tamura and Yorino (1987) and Hamdan and Nayfeh (1989) to investigate the stability of a single-machine-quasi-infinite busbar system.

In power system dynamics attention is focused sometimes on a single machine. For convenience and simplicity the rest of the system is represented by an infinite busbar where the voltage and frequency are assumed to be constant. The dynamics of the machine itself can be represented in varying degrees of detail. If the machine is represented by a classical representation (a fixed voltage behind a transient reactance), then the single machine infinite busbar system is reduced to a second-order differential equation with constant coefficients. The resulting swing equation does not offer much information about the response of the machine (Anderson and Fouad, 1977). The classical swing equation is analogous to the equation describing a harmonic oscillator.

Tamura et al. (1984,1987) introduced an innovative concept of a quasi-infinite busbar, where the rest of the system is represented by a busbar whose voltage is modulated in magnitude and phase. They formulated the problem as a Mathieu equation with both parametric and external excitations. Hamdan and Nayfeh (1989) enhanced the concept of a quasi-infinite busbar by extending the formulation to include quadratic and cubic nonlinearities. The formulation includes both parametric and external excitations. The new formulation makes it possible to apply the techniques of perturbation theory to the single-machine-quasi-infinite busbar system.

The swing equation that describes the motion of the rotor of the machine in Figure 1 can be written as (Anderson and Fouad, 1977; Pai, 1981; Tamura et al., 1984, 1987)

$$\frac{2H}{\omega_R} \frac{d^2\theta}{dt^2} + D \frac{d\theta}{dt} = P_m - \frac{V_G V_B}{X_G} \sin(\theta - \theta_B) \quad (1.1)$$

where

$$V_B = V_{B0} + V_{B1} \cos(\Omega t + \phi_v) \quad (1.2)$$

$$\theta_B = \theta_{B0} + \theta_{B1} \cos(\Omega t + \phi_\theta) \quad (1.3)$$

Here, θ is the rotor angle measured with respect to a synchronously rotating reference frame moving with constant angular velocity ω_R , H is the inertia constant of the machine, D is the damping, and P_m is the mechanical power

input to the machine. The sinusoidal term in equation (1.1) corresponds to the electrical power output of the machine, V_G is the voltage of the machine, X_G is the transient reactance of the machine, V_B is the voltage of the bus, and θ_B is the phase of the bus. For an infinite busbar, $V_{B1} = 0$ and $\theta_{B1} = 0$, whereas for a quasi-infinite busbar, V_{B1} and $\theta_{B1} \neq 0$. The magnitudes of V_{B1} and θ_{B1} are assumed to be small. The introduction of the time-varying components of the voltage and phase of the infinite busbar in equations (1.2) and (1.3) enriches the dynamics of the machine considerably.

The complex behavior of the machine for a given resonance can be studied by digital-computer simulation; that is, numerically integrating equations (1.1)-(1.3). The newly developed concepts in nonlinear dynamics can be used to interpret the results of the simulation. But even for this low-order system, which is a second-order differential equation coupled to two algebraic equations, the simulation requires a lot of time and effort. This is especially true if a parametric study is to be undertaken to assess the effect of the various parameters on the response. Thus, it is desirable to resort to any method that reduces the amount of time and effort needed to understand the behavior of the system. Such methods need not supplant simulation but they can supplement it. It is with this rationale that we are interested in approximate closed-form analytical solutions of equations (1.1)-(1.3).

We use digital-computer simulations to exhibit some of the complicated responses of the machine, including period-doubling bifurcations, chaotic

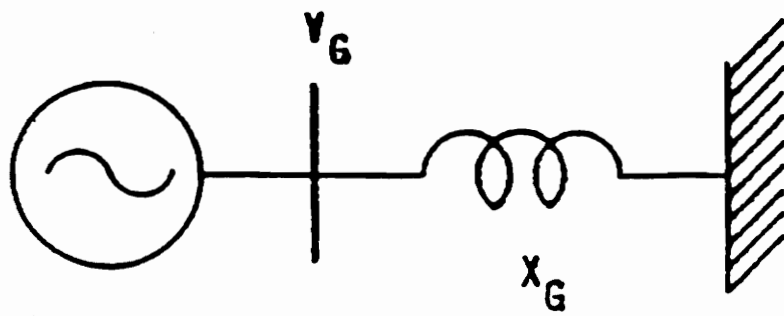


Figure 1. Single machine quasi-infinite busbar system

motions, and unbounded motions (loss of synchronism) ¹. To predict the onset of these complicated behaviors, we use the method of multiple scales (Nayfeh, 1973,1981) to develop approximate closed-form expressions for the periodic responses of the machine. Then, we use various techniques to determine the stability of the analytical solutions. The analytically predicted periodic solutions and conditions for their instability are in good agreement with the digital-computer results.

1.1 Formulation

To carry out a perturbation analysis, we find it convenient to apply the following transformation:

$$\theta - \theta_B = \delta_0 + \eta \quad (1.4)$$

Thus,

$$\delta_0 = \theta_0 - \theta_{B0} \text{ and } \eta = \Delta\theta - \theta_{B1} \cos(\Omega t + \phi_\theta) \quad (1.5)$$

where θ_0 is the operating value of θ around which the variation $\Delta\theta$ takes place. Substituting equations (1.4) and (1.5) into equations (1.1)-(1.3), expanding $\sin(\delta_0 + \eta)$ in a Taylor series around $\delta = \delta_0$, and retaining terms up to third order, we obtain the following modified swing equation:

¹ If the relative rotor angle increases indefinitely (diverges) then synchronism is lost.

$$\begin{aligned} \frac{d^2\eta}{dt^2} + \frac{\omega_R D}{2H} \frac{d\eta}{dt} + K\eta = \alpha_2\eta^2 + \alpha_3\eta^3 \\ + F_1\eta \cos(\Omega t + \phi_v) + F_2\eta^2 \cos(\Omega t + \phi_v) + F_3\eta^3 \cos(\Omega t + \phi_v) \\ + G_1 \cos(\Omega t + \phi_\theta) + G_2 \sin(\Omega t + \phi_\theta) + G_3 \cos(\Omega t + \phi_v) \end{aligned} \quad (1.6)$$

where the parameters K , α_2 , α_3 , F_1 , F_2 , F_3 , G_1 , G_2 , and G_3 are defined in Appendix A. The external excitations in equation (1.6) can be combined into a single external excitation term as follows:

$$\begin{aligned} G \cos(\Omega t + \phi_e) = G_1 \cos(\Omega t + \phi_\theta) + G_2 \sin(\Omega t + \phi_\theta) \\ + G_3 \cos(\Omega t + \phi_v) \end{aligned} \quad (1.7)$$

Equation (1.6) can be rewritten as

$$\begin{aligned} \frac{d^2\eta}{dt^2} + \frac{\omega_R D}{2H} \frac{d\eta}{dt} + K\eta = \alpha_2\eta^2 + \alpha_3\eta^3 + F_1\eta \cos(\Omega t + \phi_v) \\ + F_2\eta^2 \cos(\Omega t + \phi_v) + F_3\eta^3 \cos(\Omega t + \phi_v) + G \cos(\Omega t + \phi_e) \end{aligned} \quad (1.8)$$

The time-varying coefficients multiplying η , η^2 , and η^3 in equation (1.8) represent the multiplicative part of the excitation, which is called a parametric excitation. The inhomogeneous term $G \cos(\Omega t + \phi_e)$ represents the additive part of the excitation, which is called the effective external excitation. The solutions of equation (1.8) depend on the external excitation G , the parametric excitations represented by F_1 , F_2 , F_3 , and the relation between the frequency Ω and the linear natural frequency $\omega_0 = \sqrt{K}$.

A resonance occurs when a small excitation leads to a large response in η . The strongest parametric resonance occurs when $\Omega \simeq 2\omega_0$, which is the principal parametric resonance. The external resonance is either primary if $\Omega \simeq \omega_0$ or secondary if $m\Omega \simeq n\omega_0$, where m and n do not have common factors. If $m = 1$ and $n > 1$ then the resonance is subharmonic and if $n = 1$ and $m > 1$ the resonance is superharmonic. If both m and n are > 1 then the resonance is ultrasubharmonic (Nayfeh and Mook, 1979). We will use the method of multiple scales (Nayfeh, 1973,1981) to treat the cases of primary resonance (i.e., $\Omega \simeq \omega_0$) and of simultaneous principal parametric resonance and subharmonic resonance of order one-half (i.e., $\Omega \simeq 2\omega_0$).

1.2 Free Oscillation

Depending on the excitation amplitude and frequency and the initial conditions, equations (1.1)-(1.3) may possess bounded periodic or chaotic steady-state solutions or it may possess unbounded solutions.

The free undamped vibration of the machine is given by

$$\frac{d^2\theta}{dt^2} - \frac{\omega_R P_m}{2H} + \frac{\omega_R V_G V_{B0}}{2HX_G} \sin(\theta - \theta_{B0}) = 0 \quad (1.9)$$

where D , V_{B1} , and θ_{B1} have been set to zero in equations (1.1)-(1.3). In the interval $[-\pi, \pi]$, there are two equilibrium positions: $\theta = \theta_0$ and $\theta = \pi - \theta_0$,

where $\theta_0 < \pi - \theta_0$. The equilibrium position $\theta = \theta_0$ is a center, which is stable, and the equilibrium position $\theta = \pi - \theta_0$ is a saddle, which is unstable. A phase portrait of the solutions of equation (1.9) is shown in Figure 2a. If the initial conditions lie inside the homoclinic orbit (i.e., the closed part of the separatrix that starts and ends at the saddle point) the response of the machine will be a bounded periodic motion. However, if the initial conditions lie outside the homoclinic orbit, the response of the machine will be unbounded and hence loss of synchronism will occur.

Including the damping term in equations (1.1)-(1.3), one finds that the free motion of the machine is governed by

$$\frac{d^2\theta}{dt^2} + \frac{\omega_R D}{2H} \frac{d\theta}{dt} - \frac{\omega_R P_M}{2H} + \frac{\omega_R V_G V_{B0}}{2HX_G} \sin(\theta - \theta_{B0}) = 0 \quad (1.10)$$

In this case the phase plane is modified as shown in Figure 2b. The equilibrium points do not change; however, $\theta = \theta_0$ becomes a focus rather than a center. In this case the homoclinic orbit is destroyed. If the initial conditions lie inside the region formed by the separatrices that flow into the saddle, the response of the machine will decay to zero. On the other hand, if the initial conditions lie outside this region, the response of the machine will grow quickly and loss of synchronism will occur.

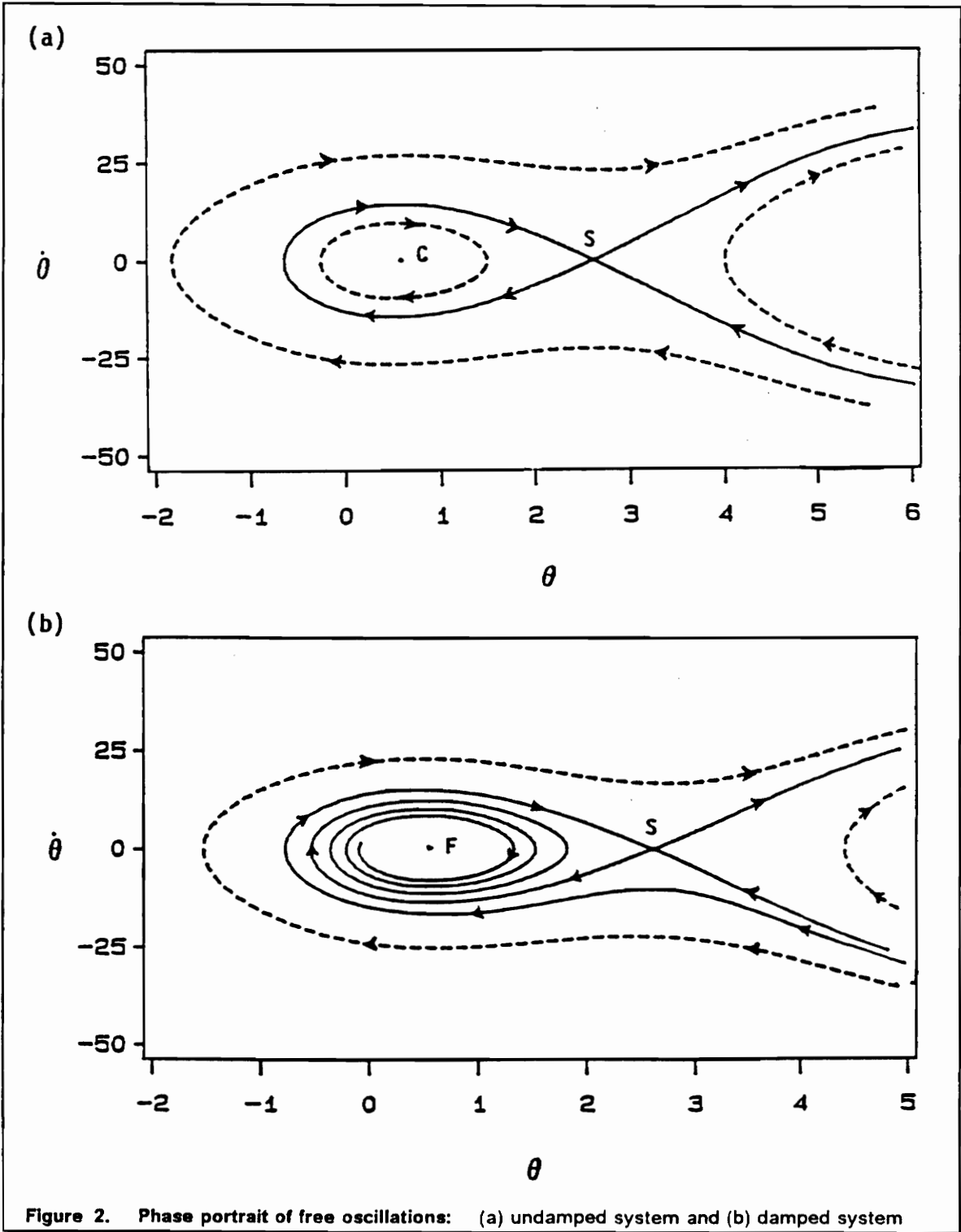


Figure 2. Phase portrait of free oscillations: (a) undamped system and (b) damped system

CHAPTER 2

Relevant Concepts of Nonlinear Dynamics

The equations describing the dynamics of a power system are nonlinear differential and algebraic equations as shown by Varaiya, Wu and Chen (1985). The equations can be linearized only under the assumption that all variables undergo small variations around an operating point. The linear analysis is indispensable for understanding the dynamical phenomena of power systems; however, the linearized system cannot capture all of the phenomena that occur in real power systems. Power systems are rich with complicated dynamics that can be explained by qualitative and geometrical methods of nonlinear analysis (Chiang, Hirsch, and Wu, 1988; Zaborsky, Huang, Zheng, and Leung, 1988). With this in mind, the following sections provide an overview of some of the basic concepts and definitions regarding the solutions of nonlinear ordinary-differential equations.

A typical system studied is modeled by a set of n first-order autonomous ordinary-differential equations of the form

$$\frac{dx}{dt} = f(x; \gamma) \quad x(t_0) = x_0 \quad (2.1)$$

where $t \in [t_0, \infty)$, $x \in \mathbb{R}^n$, $f: \mathbb{R}^n \times \mathbb{R} \rightarrow \mathbb{R}^n$ is a smooth vector field, and $\gamma \in \mathbb{R}$ is a bifurcation (control) parameter of the system. We assume that the system is *dissipative*; that is, its phase space (the space defined by displacement vs. velocity) is continuously contracting with increasing time (i.e., $\nabla \cdot f < 0$) (Lichtenberg and Lieberman, 1983). The contraction leads to a surface of lower dimension than the original phase space. The solution of equation (2.1) at time t with the initial conditions x_0 is the trajectory or flow $\phi_t(x_0)$ (Mees, 1981). We are interested in the asymptotic behavior of the solutions of equation (2.1) (i.e., the behavior of ϕ_t as $t \rightarrow \infty$).

An *attractor*, loosely speaking, is a region in the phase space which the flow of equation (2.1) approaches asymptotically (Lichtenberg and Lieberman, 1983). There is no universally accepted definition of an attractor. Lanford (1981) gave the following definition:

A subset X of the phase space is an attractor if

- a. X is invariant under the flow.
- b. There is an (open) neighborhood around X that shrinks down to X under the flow.
- c. No part of X is transient.
- d. X cannot be decomposed into two nonoverlapping invariant pieces.

The set of states in the phase space that approach X asymptotically is called the *basin of attraction*. The different types of attractors discussed in this work are equilibrium points, limit cycles, tori, and chaotic attractors.

2.1 Equilibrium Points

A point $x_e \in \mathbb{R}^n$ is called an *equilibrium point* of equation (2.1) if

$$f(x_e; \gamma) = 0 \quad \text{for } t \geq 0 \quad (2.2)$$

The stability of an equilibrium point can be determined in many cases by linearizing the flow around this equilibrium point. Thus, we let

$$x(t) = x_e + \xi(t) \quad (2.3)$$

where $\xi(t)$ is a small perturbation. Then, equation (2.1) becomes

$$\dot{x}_e + \dot{\xi} = f(x_e; \gamma) + Df(x_e; \gamma)\xi + \dots \quad (2.4)$$

where $Df = \left[\frac{\partial f_i}{\partial x_j} \right]$ is the Jacobian of $f(x; \gamma)$. Neglecting nonlinear terms, we obtain from equations (2.2) and (2.4) the variational equation

$$\dot{\xi} = Df(x_e; \gamma)\xi \quad (2.5)$$

Equation (2.5) is a system of n linear ordinary-differential equations with constant coefficients, which possess solutions of the form $x(t) = r \exp(\mu t)$ where r is a constant vector and μ is an eigenvalue of the Jacobian matrix. Hence, for an equilibrium point of (2.1) to be *asymptotically stable*, the perturbation ξ must decay to zero as $t \rightarrow \infty$; that is, if and only if

$$\operatorname{Re}(\mu_i) < 0 \quad \text{for } i = 1, 2, \dots, n \quad (2.6)$$

An equilibrium point x_e with $\operatorname{Re}(\mu_i) = 0$ while the remaining $\operatorname{Re}(\mu_i) < 0$ is usually called *neutrally stable*; a nonlinear analysis is needed to determine the stability for a neutrally stable system. An equilibrium point with $\operatorname{Re}(\mu_i) > 0$ for all i is called *unstable*. An equilibrium point with some $\operatorname{Re}(\mu_i) < 0$ and the other $\operatorname{Re}(\mu_j) > 0$ is called *non-stable* (Hirsch and Smale, 1974).

2.1.1 Bifurcations of Equilibrium Points

As the control parameter γ is varied, the value for which the flow of equation (2.1) experiences a qualitative change is called a *bifurcation point* (Sanchez, 1989). We are only concerned with codimension one bifurcations or bifurcations due to varying one parameter of the system. Equilibrium points may undergo one or more of the following three types of bifurcations (Thompson and Stewart, 1986; Seydel, 1988): *saddle-node*, *pitchfork*, and *Hopf bifurcations*.

The *saddle-node (turning point)* occurs when a real eigenvalue of the Jacobian matrix crosses the imaginary axis along the real axis into the right-half of the complex plane. Geometrically, this is seen when stable and unstable equilibrium points coalesce and annihilate each other, resulting in the solution of equation (2.1) jumping to another equilibrium point or to infinity in the phase space. This can be seen in Figure 3a.

The *pitchfork bifurcation* is similar to the saddle-node bifurcation in that it occurs when a real eigenvalue crosses the imaginary axis along the real axis into the right-half plane; however, it occurs in symmetric systems (i.e., systems that are invariant under linear transformations). The *pitchfork bifurcation* results in either two equilibrium points annihilating each other or two new equilibrium points being created. There are two types of pitchfork bifurcations: *supercritical* (Figure 3b) and *subcritical* (Figure 3c) *pitchfork bifurcations*.

Both the saddle-node and pitchfork bifurcations are static or stationary (steady-state) bifurcations (the system goes from one type of equilibrium to another). A bifurcation where a state of equilibrium gives rise to a periodic oscillation is called a *Hopf bifurcation*. A Hopf bifurcation occurs when two complex conjugate eigenvalues transversely (with nonzero speed) cross the imaginary axis into the right half-plane. A theorem postulated by Hopf in 1942 is summarized by Carr (1981) as

Assume

- a. $f(x_h, \gamma_h) = 0$.
- b. $Df(x_h; \gamma_h)$ has a simple pair of purely imaginary eigenvalues $\mu(\gamma_h) = \pm i\beta$ and no other eigenvalue with a zero real part.
- c. $\frac{d}{d\gamma} [\text{Re}(\mu)] \neq 0$.

Then there is a birth of limit cycles at (x_h, γ_h) . The initial period is $T_h = \frac{2\pi}{\beta}$.

A Hopf bifurcation could be either supercritical or subcritical. The supercritical case involves a stable equilibrium point losing stability giving way to stable periodic oscillations, and leaving an unstable equilibrium point in its place (Figure 3d). A subcritical Hopf bifurcation occurs when an unstable equilibrium gives rise to unstable periodic oscillations, leaving a stable equilibrium point in its place (Figure 3e).

2.2 Limit Cycles

A *limit-cycle* solution of equation (2.1) corresponds to a periodic oscillation.

In other words, given a solution $x(t)$ of equation (2.1), if

$$x(t) = x(t + T) \tag{2.7}$$

then $x(t)$ is a limit cycle with T being its period of oscillation. In the phase plane this corresponds to a closed trajectory. To determine the local stability

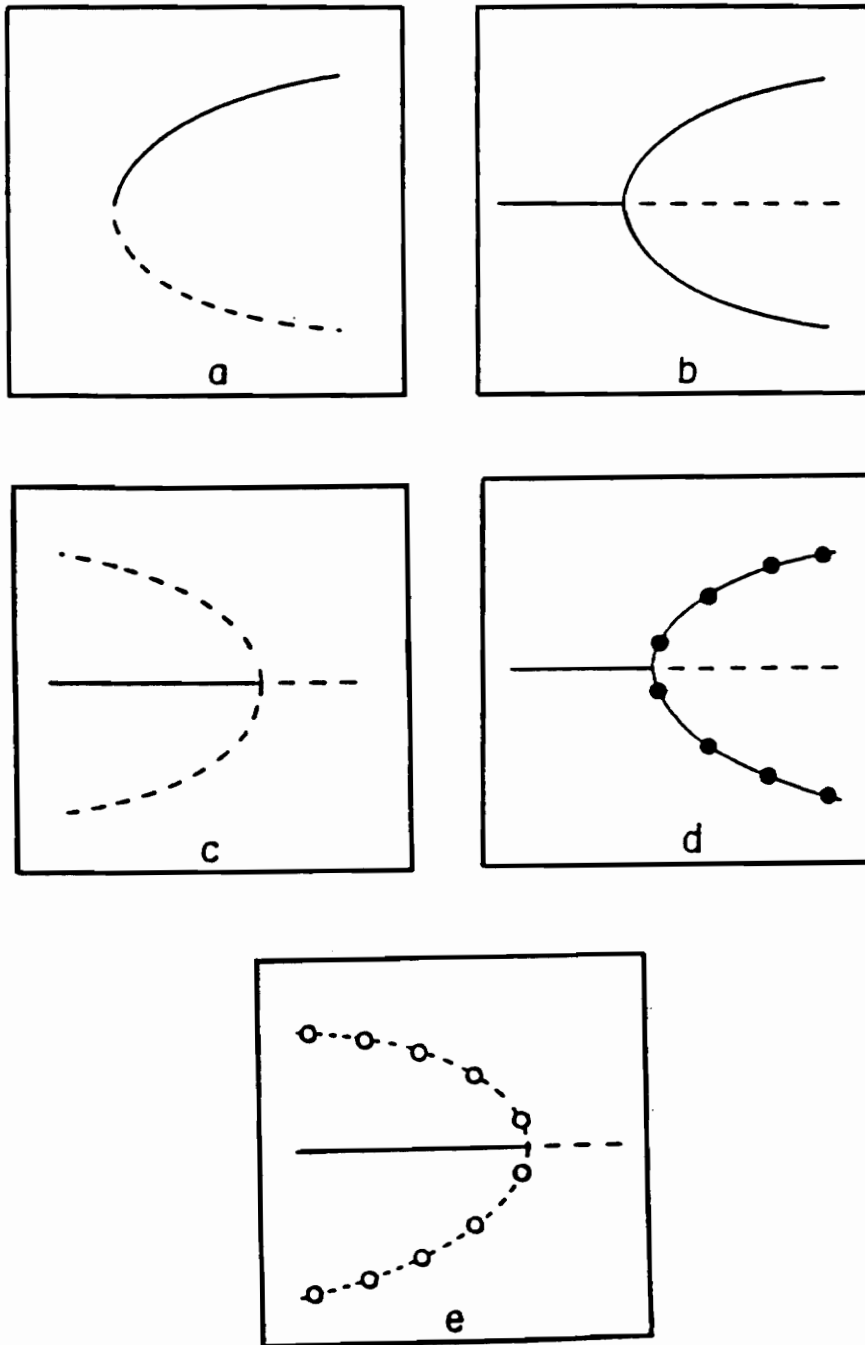


Figure 3. Bifurcation patterns: The figures represent solutions (vertical axis) versus a bifurcation parameter γ (horizontal axis); (—) stable and (---) unstable equilibrium points, solid (empty) circles represent stable (unstable) limit cycles. (Raouf, 1989).

of a limit-cycle solution $X(t)$, which has a period T , we superimpose on it a small disturbance $\xi(t)$ and obtain

$$x(t) = X(t) + \xi(t) \quad (2.8)$$

The stability of $X(t)$ depends on whether $\xi(t)$ decays or grows as $t \rightarrow \infty$.

Substituting equation (2.8) into equation (2.1), we obtain

$$\dot{\xi}(t) = f[X(t) + \xi(t); \gamma] - f[X(t); \gamma] \quad (2.9)$$

Expanding the right-hand side of equation (2.9) in a Taylor series for small $\xi(t)$ and keeping only linear terms, we obtain the variational equation

$$\dot{\xi}(t) = Df(X; \gamma)\xi(t) \quad (2.10)$$

where $Df(X; \gamma) = \frac{\partial f_i}{\partial x_j}(X; \gamma)$. Equation (2.10) is a set of n linear ordinary-differential equations with periodic coefficients having the period T .

The growth or decay of $\xi(t)$ with t is determined from Floquet theory. If $\xi(t)$ is an n -dimensional solution vector of equation (2.10), then $\xi(t + T)$ is also a solution of equation (2.10). Consequently, if Φ_t is a fundamental matrix solution (the columns of Φ_t are n linear independent vector solutions $\xi_i(t)$ of equation (2.10)), then

$$\Phi_{t+T} = \mathbf{A}\Phi_t \quad (2.11)$$

where \mathbf{A} is called the *Monodromy matrix*, which is a matrix of constant coefficients. It can be determined by calculating n linearly independent solutions $\xi_i(t)$ by integrating equation (2.10) over the interval $[0, T]$ with the initial conditions $\Phi_0 = \mathbf{I}$; hence, $\mathbf{A} = \Phi_T$. The behavior of the $\xi_i(t)$ and hence the stability of $X(t)$ depends on the eigenvalues (Floquet multipliers) of \mathbf{A} . To show this, we introduce the similarity transformation (Nayfeh and Mook, 1979)

$$U(t) = \mathbf{P}\Phi_t \quad (2.12)$$

where \mathbf{P} is a nonsingular matrix. Introducing equation (2.12) into equation (2.11) leads to

$$U(t + T) = \mathbf{P}\mathbf{A}\mathbf{P}^{-1}U(t) = \mathbf{B}U(t) \quad (2.13)$$

where \mathbf{P} can be chosen so that \mathbf{B} is a Jordan canonical form. We note that the eigenvalues of \mathbf{B} are the same as the eigenvalues of \mathbf{A} because of the similarity transformation. It should be noted that one of the Floquet multipliers always equals unity for an autonomous system (Parker and Chua, 1989).

For the case of distinct eigenvalues μ_i , we can rewrite equation (2.13) as

$$u_i(t + T) = \mu_i u_i(t), \quad i = 1, \dots, n \quad (2.14)$$

It follows from equations (2.14) that

$$u_i(t + mT) = \mu_i^m u_i(t), \quad i = 1, \dots, n \quad (2.15)$$

where m is an integer. Hence, if all of the $|\mu_i| < 1$, u_i and hence ξ_i tend to zero as $m \rightarrow \infty$ (i.e., $t \rightarrow \infty$). Consequently, the limit cycle $X(t)$ is stable (attracting). If at least one of the $|\mu_i| > 1$, the limit cycle is unstable (repelling). These stability conditions also apply to repeated Floquet multipliers (Nayfeh and Mook, 1979, pp.279-283).

2.2.1 Bifurcation of Limit Cycles

A bifurcation of a limit cycle is called an orbital bifurcation and occurs when the limit-cycle undergoes a qualitative change. As the control parameter γ is varied, a bifurcation of the limit cycle is associated with a Floquet multiplier leaving the unit circle. There are four types of orbital bifurcations: *cyclic-fold (saddle-node)*, *symmetry-breaking (pitchfork)*, *period-doubling (flip)*, and *secondary Hopf bifurcations* (Thompson and Stewart, 1986).

The type of bifurcation that occurs depends on how the Floquet multipliers leave the unit circle. If a Floquet multiplier leaves the unit circle through $+1$, a *symmetry-breaking or cyclic-fold bifurcation* occurs. The symmetry breaking bifurcation is associated with a symmetric limit cycle losing stability to asymmetric limit cycles (the unstable limit cycle continues to exist after the bifurcation). The cyclic-fold bifurcation is a result of stable and unstable limit cycles colliding, giving rise to a new attractor in the phase space. The cyclic-fold bifurcation occurs in systems with asymmetric limit cycles. If a Floquet multiplier leaves the unit circle through -1 , a *period-doubling (flip)*

bifurcation occurs. It follows from equation (2.14) that when $\mu_i = -1$, $u(t + 2T) = u_i(t)$. Thus, a solution with a period of $2T$ has been created. If two complex conjugate Floquet multipliers leave the unit circle, a *secondary Hopf bifurcation* occurs, which is usually associated with the creation of a two-period quasi-periodic (2-torus) attractor.

2.3 Torus or Quasi-periodic Attractors

A *quasi-periodic* function whose time variation is characterized by two or more incommensurate frequencies (Berge et. al., 1984). The solution of equation (2.1) associated with a quasi-periodic function is defined on a *r-torus*, where r is the number of incommensurate frequencies. We did not observe any quasi-periodic responses because we considered the case of a single-degree-of-freedom system, which does not permit this type of attractor. Two or more degrees of freedom are needed for incommensurable frequencies to exist.

2.4 Chaotic or Strange Attractor

An attracting set, which is not an equilibrium point, a limit cycle, or a torus is called a *chaotic attractor*. A Chaotic attractor is characterized as having a

fractal dimension, being sensitive to initial conditions, and whose corresponding flow has a broadband power spectrum (Moon, 1987). Strange attractors are not smooth surfaces or manifolds, they are fractal (i.e., have infinitely many-layered structures). Usually, the term strange is used to describe an attractor's geometrical nature, while the term chaotic is used to describe the motion on strange attractors. It should be noted that chaotic attractors do not exist in continuous systems of order less than three. The following sections describe different tools used to identify chaos.

2.4.1 Dimension

Equilibrium points, limit cycles, and tori all have integer dimensions. An equilibrium point has dimension zero, a limit cycle has dimension one, and an r -torus has dimension r . As mentioned earlier, chaotic attractors are not smooth surfaces or manifolds but fractal in nature and one speaks of a fractal dimension (Mandelbrot, 1982).

A commonly used definition of dimension is the Hausdorff dimension. Suppose that $N(\varepsilon)$ is the number of small n -dimensional cubes of side length ε that are required to cover the attractor. Then, the *dimension or Hausdorff dimension* is defined as

$$D = \lim_{\varepsilon \rightarrow 0} \frac{\ln(N(\varepsilon))}{\ln(1/\varepsilon)} \quad (2.16)$$

2.4.2 Liapunov Exponents and Dimension

A useful tool for distinguishing the various types of attractors (equilibrium points, limit cycles, tori, chaotic attractors) consists of the determination of the *Liapunov exponents*. The Liapunov exponents are related to the rate of divergence or convergence of trajectories corresponding to initial conditions arbitrarily close to one another. The Liapunov exponents are related to the Floquet multipliers because they are also obtained from the variational equation (2.1). Parker and Chua (1989) define the *Liapunov exponents* as

$$\lambda_i = \lim_{t \rightarrow \infty} \left[\frac{1}{t} \ln | \mu_i(t) | \right] \quad (2.17)$$

where the $\mu_i(t)$ are the eigenvalues of Φ_t . There are n Liapunov exponents for an n -dimensional system. We note that one of the n -exponents will always be equal to zero for an autonomous system. For a dissipative system, $Df < 0$ and the sum of the Liapunov exponents is always less than zero, hence the flow is always contracting, and the volume occupied by an attractor is zero.

Using Liapunov exponents to characterize the asymptotic behavior of the system (Parker and Chua, 1989), we have

Stable equilibrium point: $\lambda_i < 0$, for $i = 1, \dots, n$

Stable limit cycle: $\lambda_1 = 0$ and $\lambda_i < 0$ for $i = 2, \dots, n$

Stable r-torus: $\lambda_1 = \dots = \lambda_r = 0$, and $\lambda_i < 0$ for $i = r + 1, \dots, n$

A chaotic attractor is characterized by having at least one Liapunov exponent being positive. Because the sum of the Liapunov exponents for a dissipative system is less than zero and one of the Liapunov exponents is always zero for an autonomous system, chaos does not exist in autonomous dissipative systems of order less than three. The consequence of the presence of a positive Liapunov exponent is that the chaotic attractor is sensitive to initial conditions.

Another commonly used dimension is the Liapunov dimension defined by Frederickson et al.(1983) as

$$D_l = j + \sum_{i=k}^j \frac{\lambda_k}{|\lambda_{j+1}|} \quad (2.18)$$

where the λ_i are ordered such that $\lambda_n > \lambda_{n-1} > \dots > \lambda_2 > \lambda_1$, and j is the largest integer such that

$$\sum_{k=1}^j \lambda_k > 0 \quad (2.19)$$

Wolf et al. (1984) and Parker and Chua (1989) developed algorithms to compute the Liapunov exponents from experimental data and numerical simulations, respectively. Grebogi et al. (1984) showed that a fractal Liapunov dimension indicates a strange attractor and not a chaotic attractor. Moreover, strange attractors are usually chaotic but this is not always the case.

2.4.3 Sensitivity to Initial Conditions

A chaotic system is unpredictable. Any two distinct initial conditions arbitrarily close to one another on the attractor will diverge with time, resulting in two trajectories with no correlation between them. The chaotic systems' property of amplifying errors or initial uncertainties is called *sensitivity to initial conditions*.

2.4.4 Power Spectrum

Another method of characterizing a chaotic attractor is by its power spectrum. An equilibrium point is characterized by having only a dc component. A limit cycle is characterized by discrete peaks at the fundamental frequency and its harmonics. A quasi-periodic attractor is characterized by peaks at its fundamental frequencies, their harmonics, and combinations. A chaotic attractor is characterized by a broadband power spectrum.

2.4.5 Transitions to Chaos

So far we have described various types of bifurcations as the parameter γ is varied. In this work, we are also interested in the values of γ which result in chaotic attractors. Three possible routes to chaos (Berge et al., 1984) have been identified in the literatures: via *torus bifurcation*, *period-doubling bifurcations*, and *intermittency*. We only observed the period-doubling route to chaos.

2.4.5.1 Torus Bifurcation Route to Chaos

Newhouse, Ruelle, and Takens (1978) proposed that chaos can arise after a finite number of secondary Hopf bifurcations. This is in contrast with Landau (1944) who proposed that an infinite number of secondary Hopf bifurcations are needed for a chaotic attractor to occur. The proposition of Newhouse et al. has been proven both experimentally and numerically, while Landau's proposition has not. Schematically, Newhouse et al. proposition can be described as follows: suppose a control parameter is increased resulting in the equilibrium point losing stability and giving rise to a stable periodic oscillation with frequency f_1 . Then two secondary Hopf bifurcations occur resulting in the creation of two new frequencies f_2 and f_3 . The system is now a 3-torus, which they showed leads to a chaotic attractor because the 3-torus is inherently unstable.

2.4.5 Transitions to Chaos

So far we have described various types of bifurcations as the parameter γ is varied. In this work, we are also interested in the values of γ which result in chaotic attractors. Three possible routes to chaos (Berge et al., 1984) have been identified in the literatures via *torus bifurcation*, *period-doubling bifurcations*, and *intermittency*. We only observed the period-doubling route to chaos.

2.4.5.1 Torus Bifurcation Route to Chaos

Newhouse, Ruelle, and Takens (1978) proposed that chaos can arise after a finite number of secondary Hopf bifurcations. This is in contrast with Landau (1944) who proposed that an infinite number of secondary Hopf bifurcations are needed for a chaotic attractor to occur. The proposition of Newhouse et al. has been proven both experimentally and numerically, while Landau's proposition has not. Schematically, Newhouse et al. proposition can be described as follows: suppose a control parameter is increased resulting in the equilibrium point losing stability and giving rise to a stable periodic oscillation with frequency f_1 . Then two secondary Hopf bifurcations occur resulting in the creation of two new frequencies f_2 and f_3 . The system is now a 3-torus, which they showed leads to a chaotic attractor because the 3-torus is inherently unstable.

2.4.5.2 *Period-Doubling Route to Chaos*

The route to chaos we observed is through a sequence of period-doubling bifurcations (Feigenbaum, 1978). As a control parameter is varied a limit cycle of period T and frequency f loses its stability giving rise to a new limit cycle having a period that is $2T$ and a frequency that is $\frac{1}{2}f$. As the parameter is increased further, repeated period-doubling bifurcations give rise to the frequencies $\frac{1}{2}f, \frac{1}{4}f$, etc.. This process continues till it accumulates at a critical value where a broadband frequency spectrum occurs, indicating chaos.

2.4.5.3 *Intermittency*

The third route to chaos is that of intermittency. The concept of intermittency was proposed by Pomeau and Manneville (1980). Intermittency refers to oscillations that are periodic, but contain infrequent variations of large amplitudes (bursts of aperiodic oscillations of finite duration). As the system becomes chaotic the duration of the variations becomes longer.

2.5 Invariant Manifolds

An *invariant manifold* E is a subset of the phase space such that for any initial value $x_0 \in E$, the corresponding flow $\phi_t(x_0)$ will remain in E . From equation (2.10) the solution space defined by $\Phi_t(x_e)$ can be divided into three subspaces:

$$\text{center subspace: } E^c = \text{span}\{w^1, \dots, w^{n_c}\}$$

$$\text{stable subspace: } E^s = \text{span}\{v^1, \dots, v^{n_s}\}$$

$$\text{unstable subspace: } E^u = \text{span}\{u^1, \dots, u^{n_u}\}$$

where $\{w^j\}_{j=1}^{n_c}$, $\{v^j\}_{j=1}^{n_s}$, and $\{u^k\}_{k=1}^{n_u}$ are the eigenvectors corresponding to the eigenvalues with zero real parts, negative real parts, and positive real parts, respectively (Guckenheimer and Holmes, 1983). The center, stable, and unstable manifolds are invariant manifolds tangent to the center, stable, and unstable subspaces at the equilibrium point, respectively.

Invariant manifolds are used to describe the limit sets that consist of trajectories that connect saddles (non-stable equilibrium points) and nodes (unstable equilibrium points with no complex eigenvalues). A *homoclinic orbit* connects a saddle to itself and a *heteroclinic orbit* connects a saddle to another saddle (Seydel, 1988). A stable manifold approaches a saddle as $t \rightarrow \infty$ and an unstable manifold approaches a saddle as $t \rightarrow -\infty$. Determination of these manifolds is important because they give insight to the local as well as the global behavior of the system in the phase space.

2.6 Poincaré Section

In an n -dimensional autonomous system an $(n-1)$ -dimensional hypersurface Σ is said to be a *Poincaré section* if the flow lines intersect Σ transversally and in the same direction (Hirsch and Smale, 1974). The hypersurface Σ divides the phase space into two regions Σ_+ and Σ_- , where the '+' and '-' correspond to trajectories that cross Σ from the front and rear, respectively, and Σ_+ and Σ_- are called one-sided Poincaré sections. The Poincaré map has three advantages: it reduces the number of coordinates from n to $n - 1$, reduces the amount of data, and time is discretized (Eckmann and Ruelle, 1985). The points that cross Σ are related by difference equations instead of differential equations, which define the *Poincaré maps*. The hypersurface Σ is typically chosen such that the trajectories intersect it every T seconds, where T is the period of the limit cycle. Poincaré maps are useful in distinguishing among the various attractors. A single point in the map corresponds to an equilibrium point or a period-one limit cycle. Two points correspond to a period-two limit cycle. A closed curve corresponds to a 2-torus. A Poincaré map which is not one of the above may be a strange attractor.

CHAPTER 3

Primary Resonance

3.1 *Introduction*

In this chapter we concentrate on the case of primary resonance, which occurs when Ω is near ω_0 . We demonstrate using digital simulation that, for a given set of parameters of equations (1.1)-(1.3), the primary resonance leads to a complicated behavior. We show that as Ω is varied from a value above ω_0 the response is periodic, then as Ω is decreased a series of period-doubling bifurcations takes place culminating in a chaotic motion, and finally the response becomes unbounded as the machine experiences loss of synchronism.

The effect of varying a control parameter of the system is studied by forming a bifurcation diagram in a two parameter space indicating where cyclic-fold (saddle-node, tangent) instabilities and period-doubling (flip) bifurcations occur. The variation of a control parameter affects the basins of attraction, as shown by Grebogi, Ott, and Yorke (1988), Nayfeh and Sanchez (1989), and Soliman and Thompson (1989). Alternatively we use perturbation analysis to obtain a closed-form approximate solution of equations (1.1)-(1.3). We demonstrate that the period-one results obtained by numerical simulation can be obtained directly and with less effort from the perturbation solution. Moreover, we show that the instability of the closed-form solution predicts the onset of period-doubling bifurcations, which are precursors to chaos and loss of synchronism.

3.2 Numerical Simulation

Equations (1.1)-(1.3) were simulated on the digital computer by using a fifth- and sixth-order Runge-Kutta algorithm for the parameters given in Appendix B. The effect of varying the excitation frequency Ω and the initial conditions when $V_{B1} = 0.1$ was studied in detail, and representative results are shown in Figure 4.

For large Ω , there exists only one stable steady-state solution (attractor), which is periodic having the period $T = 2\pi/\Omega$. An example is shown in Figure

4a. The phase portrait of the attractor forms a closed orbit. Since it takes the period $T = 2\pi/\Omega$ to close, this attractor is called a period-one attractor. This can be verified by observing the FFT (Figure 4b) and Poincaré map (Figure 4c) of the time trace of the attractor. The FFT has discrete frequency components at the excitation frequency Ω and its harmonics and the Poincaré map has only one point. As Ω is decreased, the period-one orbit deforms and increases in size until Ω reaches the threshold value $\Omega = 8.43018$ rad/sec. As Ω is decreased further, the orbit changes qualitatively as well as quantitatively as shown in Figure 4d. Now, the orbit has two loops instead of one loop and it takes a time of $2T$ to close. The FFT (Figure 4e) of its time trace has discrete components at $\frac{1}{2}\Omega, \Omega$, and their harmonics and combination frequencies. The Poincaré map (Figure 4f) now has two points, indicating that the period of the attractor has doubled. The doubling of the system's period is a result of a period-doubling bifurcation.

As Ω is decreased further, the period-two attractor deforms and increases in size until another threshold value of $\Omega = 8.29411$ rad/sec is reached. Beyond, this value, the attractor again changes quantitatively and qualitatively, as shown in Figure 4g. The phase portrait now has four loops, the FFT (Figure 4h) has discrete components at $\frac{1}{4}\Omega, \frac{1}{2}\Omega, \Omega$, their harmonics and combination frequencies, and the Poincaré map (Figure 4i) has four points. Hence the period of the attractor has doubled again, resulting in a period-four attractor. This sequence of period-doubling bifurcations continues as Ω is decreased further and eventually culminates in a chaotic attractor, as shown

in Figure 4j. The FFT (Figure 4k) of the time trace of this chaotic attractor has a broadband character and the Poincaré map (Figure 4l) shows now a strange attractor. The corresponding Liapunov exponents are 1.4427, 0.0, and -7.69 and the Liapunov dimension is $D_l = 2.19$. As Ω is decreased even further the response of the system becomes unbounded (Figure 4m), resulting in loss of synchronism.

We note that equations (1.1)-(1.3) have another small steady-state response (attractor) having the same period as that of the excitation. This small attractor may coexist with either the large period-one attractor or its bifurcated attractors. When more than one attractor coexist, the initial conditions determine the response. The coexistence of multiple attractors is due to the nonlinearities in equation (1.1).

To understand the effect of varying the parameters on the system's response, we study the two-parameter space corresponding to the frequency Ω and amplitude V_{B1} of the external excitation. A comprehensive picture of the behavior of the nonlinear system in this space is given in Figure 5. The power system has the typical Y-shaped zones found in Grebogi et al. (1989) and Nayfeh and Sanchez (1989). Region A lies below the arm with negative slope defined as y_1 , which is where the small orbit exists. When any of the parameters are varied to cross y_1 in the direction of the arrow, a tangent (saddle-node, cyclic-fold) instability occurs. The resulting solution depends on the state of the system and the attracting set of the subsequent parameter

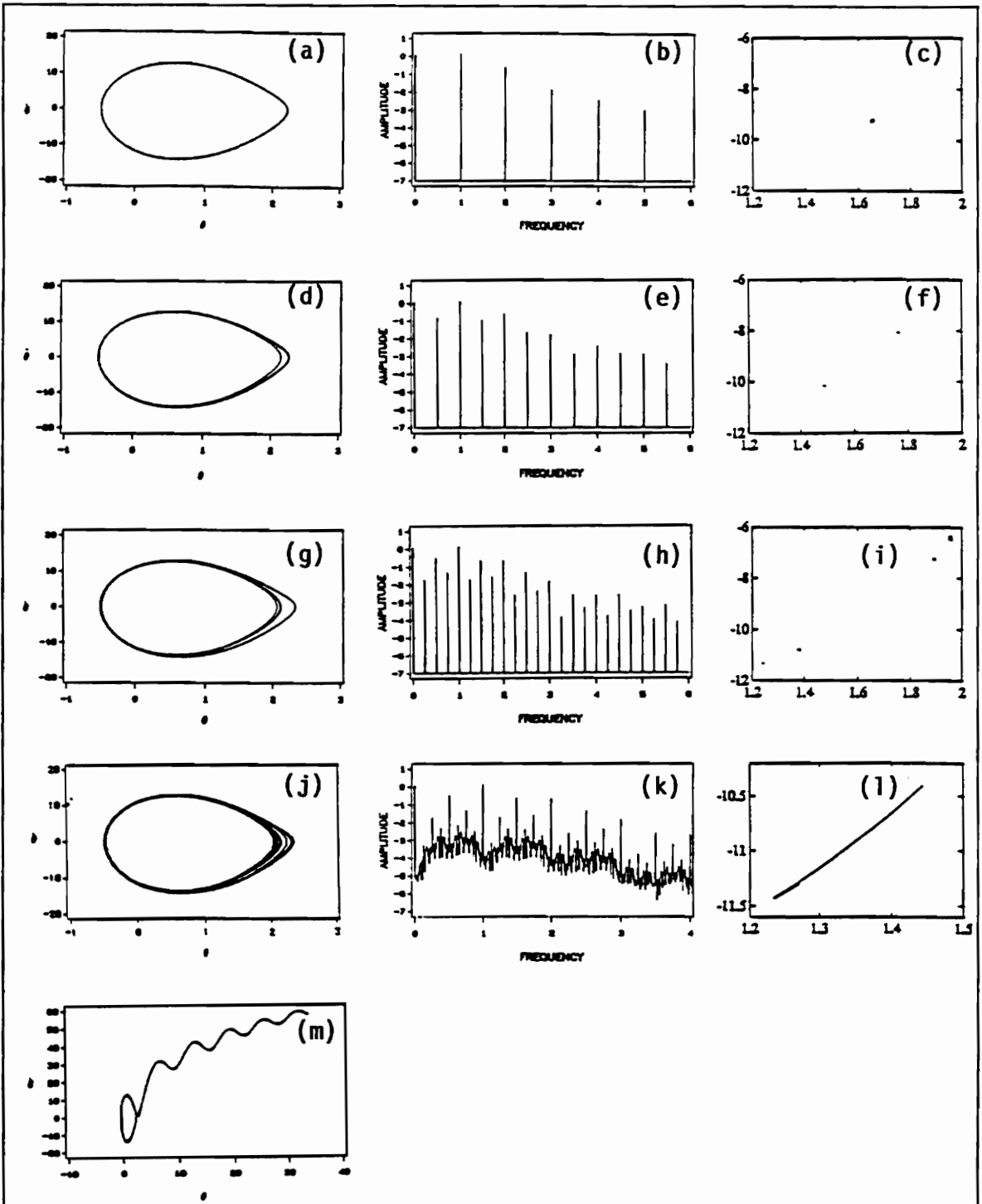


Figure 4. Numerical simulation for case of primary resonance: (a)-(c) period-one $\Omega = 8.6$ rad/sec; (d)-(f) period two $\Omega = 8.4$ rad/sec; (g)-(i) period four $\Omega = 8.28$ rad/sec; (j)-(l) chaos $\Omega = 8.27$ rad/sec; (m) loss of synchronism $\Omega = 8.26$ rad/sec.

space. If the parameters are varied to cross y_1 into region B , the small orbit loses stability and the system jumps to the large orbit, which is the attracting set in that parameter space. However, if the parameters are varied to cross y_1 into region D the small orbit loses stability, and the system's response becomes unbounded. Region B defined as the region lying under the curve y_2 ; it corresponds to the attracting set of the large attractor. The curve y_2 indicates the occurrence of the first period-doubling bifurcation. Shortly after the first period-doubling bifurcation occurs a sequence of period-doubling bifurcations occur culminating in a chaotic attractor. This region is very small and is not shown. If the parameters are varied to cross the curve y_3 into region A , then the existing attractor loses stability giving way to a small attractor and an unbounded motion otherwise.

In Region C , large and small attractors coexist. The response of the system in this region depends on the initial conditions. Usually this region would be bounded by another curve connecting y_1 and y_3 . This figure is typically given as g versus Ω , however, g is a function of V_{B1} , θ_{B1} , and the phase between them, which can be seen from equations (1.1)-(1.3). Thus, if $\theta_{B1} \neq 0$, g can be greater than zero even if $V_{B1} = 0$. For this curve to exist the amplitude g of the effective external excitation must become small enough, causing the frequency-response curve to be single-valued and the large attractor to lose stability by jumping down to the small attractor. Because $\theta_{B1} = 0.1$ rad in these simulations, we cannot obtain a single-valued frequency-response curve because the effective external excitation is not small enough for $V_{B1} = 0$.

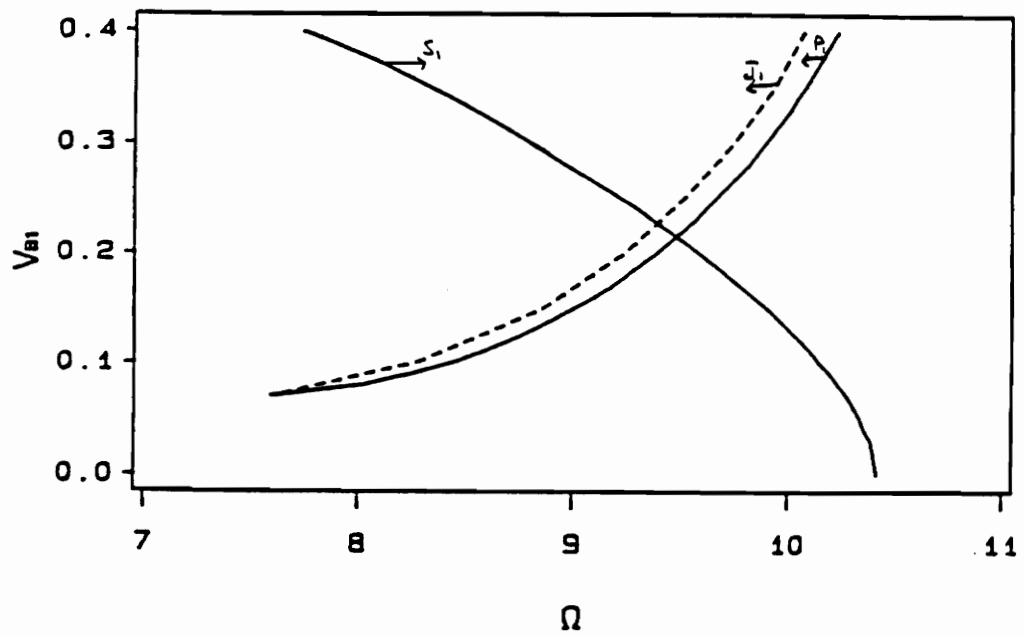


Figure 5. Bifurcation diagram for case of primary resonance

As mentioned previously, the system's response depends on the initial conditions. The chart in Figure 6 was constructed by studying the local stability of the different possible attractors; we note that some solutions may be locally stable but globally unstable. To understand the global behavior of the system, we formed a map of all the possible solutions for various initial conditions (i.e., basin of attraction). For a given set of parameters, we covered the region $-1 \leq u \leq 3.5$ and $-20 \leq \dot{u} \leq 20$ by a grid of 400x450 initial conditions. For each set of initial conditions, we integrated equations (1.1)-(1.3) for 20 cycles, sometimes 100 or 400 cycles. If the solution becomes unbounded the corresponding grid point is marked by a black dot; otherwise, it is marked by a white dot. By changing one of the system parameters, we can observe the metamorphoses that the basins of attraction undergo. Figure 6 shows a series of metamorphoses that the system undergoes as V_{B1} is varied at $\Omega = 8.26$ rad/sec.

As V_{B1} is increased past $V_{B1} = 0.06$ the smooth basin boundary begins to form fingers that corrupt the once stable region formed by the separatrices of the free oscillating system. The corrupted region becomes more complicated and possibly fractal as V_{B1} is increased as shown in Figures 6(c-h). As V_{B1} is increased further the region becomes less complicated, but the stable region becomes smaller and smaller. Nevertheless there continues to be stable regions interspersed in the unstable regions as shown in Figures 6(i-j).

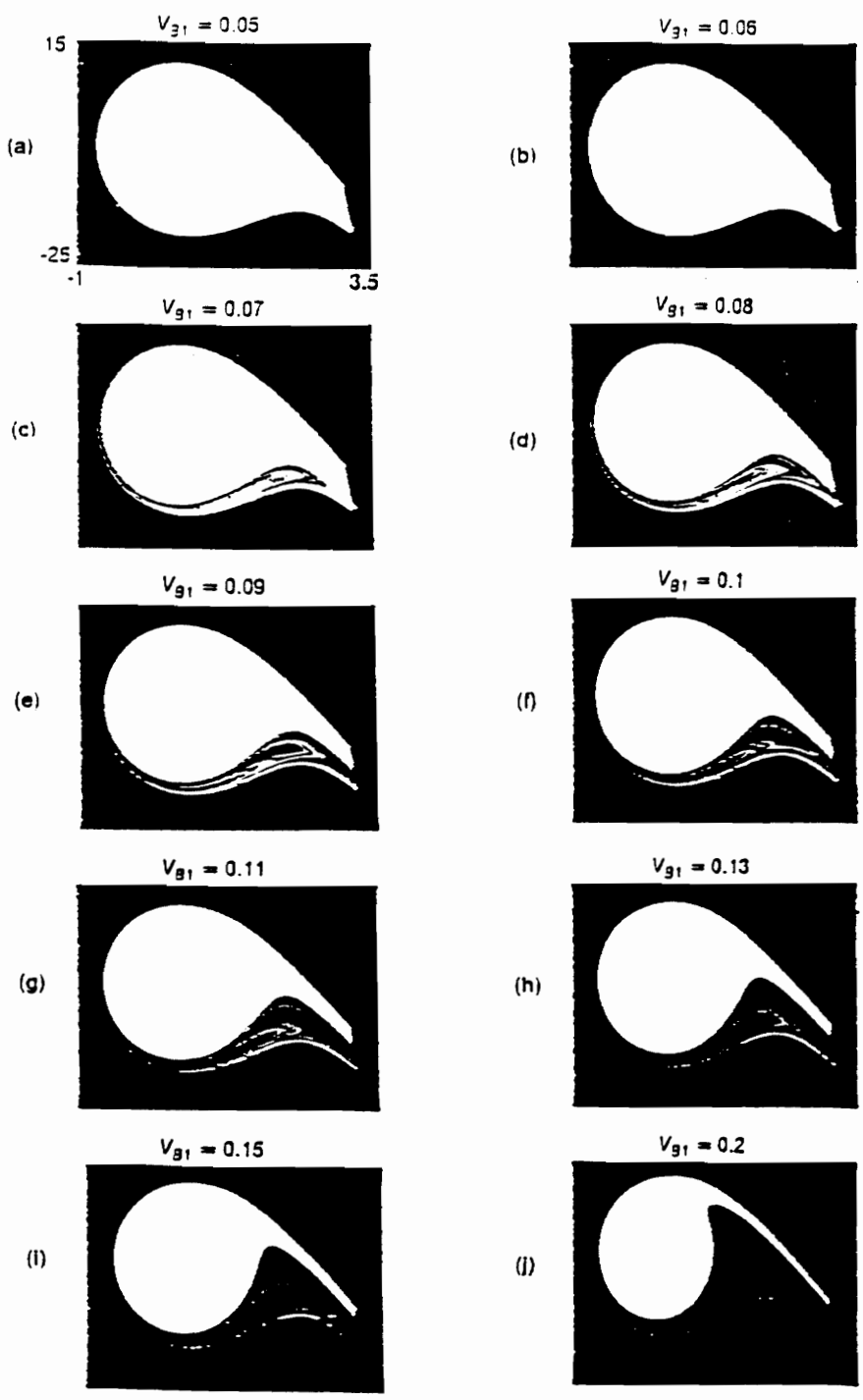


Figure 6. Basins of attraction ($\dot{\theta}$ vs. θ) for case of primary resonance: white (stable) and black (unstable).

In the next section, we show that one can develop a fairly accurate closed-form expression for the period-one attractor. Moreover, one can use this solution to predict conditions for the onset of the saddle-node and period-doubling bifurcations, which are precursors to chaos and loss of synchronism.

3.3 *Perturbation Analysis*

In this section, we concentrate on the case of primary resonance $\Omega \approx \omega_0$. We use the method of multiple scales to determine a uniform solution of equation (1.8) for the case of small but finite amplitudes (i.e., weak nonlinearities). To analyze this case we need to order the damping, the nonlinearities, and the excitation so that their effects occur at the same order. This ordering is accomplished by introducing a small dimensionless parameter ε that is used as a bookkeeping device and will be set equal to unity in the final analysis. If $\eta = 0(\varepsilon)$, then $\frac{\omega_R D}{2H} = 0(\varepsilon^2)$ and we assume that $V_{B1} = 0(\varepsilon^3)$ and $\theta_{B1} = 0(\varepsilon^3)$. With this ordering, we put

$$F_1 = \varepsilon^3 f_1, F_2 = \varepsilon^3 f_2, F_3 = \varepsilon^3 f_3, \quad \text{and } G = \varepsilon^3 g$$

Moreover, to quantitatively describe the nearness of the resonance, we introduce the detuning parameter σ defined according to

$$\omega_0^2 = \Omega^2 + \varepsilon^2 \sigma \tag{3.1}$$

Then, equation (1.8) can be rewritten as

$$\begin{aligned} \ddot{\eta} + 2\varepsilon^2\mu\dot{\eta} + (\Omega^2 + \varepsilon^2\sigma)\eta &= \alpha_2\eta^2 + \alpha_3\eta^3 + \varepsilon^3f_1\eta \cos(\Omega t + \phi_v) \\ &+ \varepsilon^3f_2\eta^2 \cos(\Omega t + \phi_v) + \varepsilon^3f_3\eta^3 \cos(\Omega t + \phi_v) \\ &+ \varepsilon^3g \cos(\Omega t + \phi_e) \end{aligned} \quad (3.2)$$

where the overdot indicates the derivative with respect to t .

We seek a uniform solution of equation (3.2) in the form

$$\eta(t; \varepsilon) = \varepsilon\eta_1(T_0, T_1, T_2) + \varepsilon^2\eta_2(T_0, T_1, T_2) + \varepsilon^3\eta_3(T_0, T_1, T_2) + \dots \quad (3.3)$$

where $T_0 = t$ is a fast scale, characterizing motions occurring at the frequencies Ω and ω_0 , and $T_1 = \varepsilon t$ and $T_2 = \varepsilon^2 t$ are slow scales, describing the modulations of the amplitude and phase with damping, nonlinearities, and resonances. In terms of these time scales, the time derivatives become

$$\frac{d}{dt} = D_0 + \varepsilon D_1 + \varepsilon^2 D_2 + \dots \quad (3.4a)$$

$$\frac{d^2}{dt^2} = D_0^2 + 2\varepsilon D_0 D_1 + \varepsilon^2 (2D_0 D_2 + D_1^2) + \dots \quad (3.4b)$$

where $D_n = \partial/\partial T_n$. Substituting equations (3.3) and (3.4) into equation (3.2) and equating coefficients of like powers of ε , we obtain

$$D_0^2\eta_1 + \Omega^2\eta_1 = 0 \quad (3.5)$$

$$D_0^2\eta_2 + 2D_0D_1\eta_1 + \Omega^2\eta_2 = \alpha_2\eta_1^2 \quad (3.6)$$

$$D_0^2 \eta_3 + 2D_0 D_1 \eta_2 + (D_1^2 + 2D_0 D_2) \eta_1 + 2\mu D_0 \eta_1 + \Omega^2 \eta_3 + \sigma \eta_1 = 2\alpha_2 \eta_1 \eta_2 + \alpha_3 \eta_1^3 + g \cos(\Omega t + \phi_e) \quad (3.7)$$

We note from equations (3.5)-(3.7) that, in this case, the effects of the parametric terms are unimportant, thus we only have an external forcing term.

The solution of equation (3.5) can be expressed in the form

$$\eta_1 = A(T_1, T_2) e^{i\Omega T_0} + \bar{A}(T_1, T_2) e^{-i\Omega T_0} \quad (3.8)$$

where A is an undetermined function at this level of approximation; it will be determined by eliminating the secular terms at the next orders of approximation. Substituting equation (3.8) into equation (3.6) yields

$$D_0^2 \eta_2 + \Omega^2 \eta_2 = -2i\Omega D_1 A e^{i\Omega T_0} + \alpha_2 [A^2 e^{2i\Omega T_0} + A\bar{A}] + cc \quad (3.9)$$

where cc is the complex conjugate of the preceding terms. In equation (3.9), $D_1 A$ has to be zero, otherwise a secular term appears in η_2 , making the expansion nonuniform for large t . Hence $A = A(T_2)$ and the solution of equation (3.9) can be written as

$$\eta_2 = -\frac{\alpha_2 A^2 e^{2i\Omega T_0}}{3\Omega^2} - \frac{\alpha_2 \bar{A}^2 e^{-2i\Omega T_0}}{3\Omega^2} + \frac{2\alpha_2 A\bar{A}}{\Omega^2} \quad (3.10)$$

Substituting equations (3.8) and (3.10) to equation (3.7) and eliminating the terms that lead to secular terms yields

$$2i\Omega(A' + \mu A) + 8\alpha_e A^2 \bar{A} - \frac{1}{2} g e^{i\phi_e} + \sigma A = 0 \quad (3.11)$$

where

$$\alpha_e = -\frac{5\alpha_2^2}{12\Omega^2} - \frac{3}{8} \alpha_3 \quad (3.12)$$

Next, we express A in the polar form

$$A = \frac{1}{2} a e^{i(\beta + \phi_e)} \quad (3.13)$$

Substituting equation (3.13) into equation (3.11) and separating real and imaginary parts, we obtain

$$\Omega(a' + \mu a) + \frac{1}{2} g \sin \beta = 0 \quad (3.14)$$

$$-\Omega a \beta' + \alpha_e a^3 - \frac{1}{2} g \cos \beta + \frac{1}{2} \sigma a = 0 \quad (3.15)$$

Therefore, to the second approximation

$$\eta = \varepsilon a \cos(\Omega t + \beta + \phi_e) + \frac{\varepsilon^2 a^2 \alpha_2}{6\Omega^2} [3 - \cos(2\Omega t + 2\beta + 2\phi_e)] + \dots \quad (3.16)$$

where a and β are given by equation (3.14) and (3.15). We can set $\varepsilon = 1$ and consider a as the perturbation parameter and thus rewrite equations (1.5) and (3.16) as



$$\begin{aligned}\Delta\theta &= \theta_{B1} \cos(\Omega t + \phi_0) + a \cos(\Omega t + \beta + \phi_e) \\ &+ \frac{a^2 \alpha_2}{6\Omega^2} [3 - \cos(2\Omega t + 2\beta + 2\phi_e)] + \dots\end{aligned}\quad (3.17)$$

Equation (3.17) shows that the excursions of the rotor from the operating point follow an oscillatory motion, which includes a drift or what is called a steady streaming (Nayfeh and Mook, 1979). The drift term $\frac{a^2 \alpha_2}{2\Omega^2}$, due to the quadratic nonlinearity, indicates a shift in the operating point so that the oscillatory motion is not centered at $\theta = \theta_0$.

To determine the character of the solutions of equations (3.14) and (3.15), we need to determine their singular or fixed points. The fixed points of equations (3.14) and (3.15) correspond to $a' = \beta' = 0$. They are given by

$$\mu a = \frac{-g \sin \beta}{2\Omega} \quad (3.18a)$$

$$\frac{a\sigma}{2\Omega} + \frac{\alpha_e a^3}{\Omega} = \frac{g \cos \beta}{2\Omega} \quad (3.18b)$$

Squaring and adding equations (3.18) yields the frequency-response equation

$$\mu^2 + \left(\frac{\sigma}{2\Omega} + \frac{\alpha_e a^2}{\Omega} \right)^2 = \frac{g^2}{4\Omega^2 a^2} \quad (3.19)$$

Equation (3.19) is an implicit equation for the amplitude a as a function of the detuning parameter σ (the frequency of the excitation) and the amplitude g of

the excitation. The plot of a as a function of Ω for a given μ and g is called a frequency-response curve (Figure 7).

3.3.1 Comparison of the Perturbation Solution with Numerical Simulations

Next, we compare the results of the second-order closed-form analytical solution with numerical simulations. The solutions of equations (3.18a) and (3.18b) are obtained numerically by using a Newton-Raphson procedure. Then η and $\dot{\eta}$ are calculated from equation (3.16). A typical time history and phase portrait are shown in Figures 8a and 8b for $\Omega = 8.6$ rad/sec.

It follows from equation (1.4) that

$$\eta = \theta - \theta_B - \delta_0 \quad (3.20)$$

$$\dot{\eta} = \dot{\theta} - \dot{\theta}_B \quad (3.21)$$

Substituting the time histories for θ and $\dot{\theta}$ obtained by the numerical simulation into equations (3.20) and (3.21), we calculate η and $\dot{\eta}$. The results for $\Omega = 8.6$ rad/sec are also shown in Figures 8a and 8b. The agreement between the closed-form analytical expression and the results of the numerical simulation is remarkable.

To compare the analytical results with the numerical simulations at other frequencies, we plot in Figure 7 the maximum values of η obtained by using

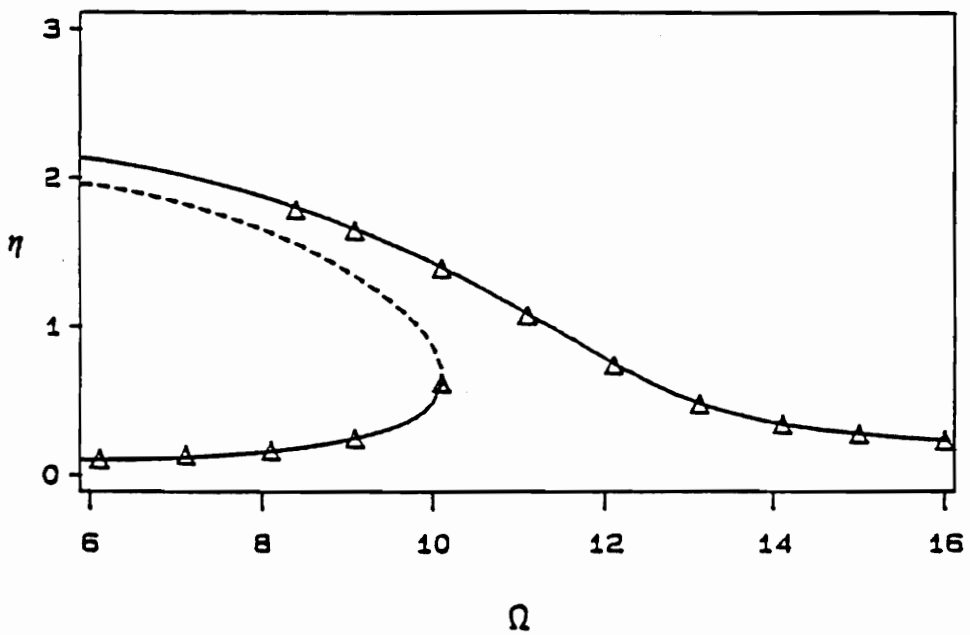
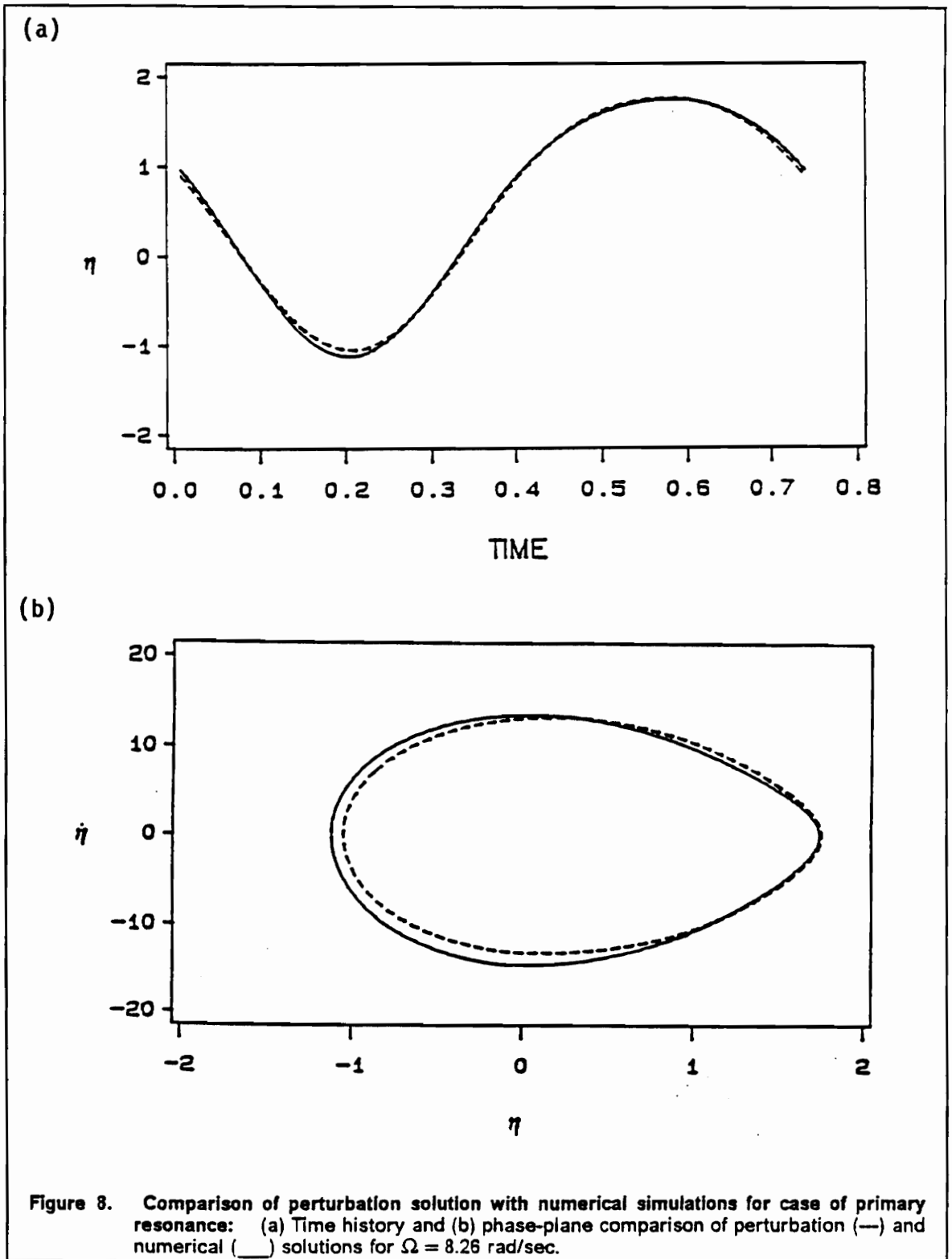


Figure 7. Frequency-response curve for case of primary resonance: perturbation solution: (—) stable, (---) unstable; numerical solution: Δ .



the two approaches. The continuous curves represent the analytical solution and the triangles represent the results of the numerical simulation. Again, the agreement between them is remarkable up to the value of Ω corresponding to the onset of period-doubling bifurcations.

3.4 Stability of Period-One Solutions

3.4.1 Floquet Theory

Different methods are used to determine the stability of the analytically predicted period-one solutions $\eta(t)$. The first method is a numerical application of Floquet theory (Nayfeh and Mook, 1979). We introduce an arbitrary small disturbance $\xi(t)$ and obtain

$$\hat{\eta}(t) = \eta(t) + \xi(t) \quad (3.22)$$

The stability of $\eta(t)$ depends on whether $\xi(t)$ decays or grows as $t \rightarrow \infty$. Substituting equation (3.22) into equation (1.8) and retaining only linear terms in $\xi(t)$, we obtain the variational equation

$$\frac{d^2\xi}{dt^2} + \frac{\omega_R D}{2H} \frac{d\xi}{dt} + (K - 2\alpha_2\eta - 3\alpha_3\eta^2)\xi = 0 \quad (3.23)$$

which is a linear differential equation with periodic coefficients having the period $T = 2\pi/\Omega$. The behavior of $\xi(t)$ with t is determined from Floquet theory. If $\xi_1(t)$ and $\xi_2(t)$ are two linearly independent solutions of equation (3.23), then $\xi_1(t + T)$ and $\xi_2(t + T)$ are also solutions of equation (3.23) and they are linear combinations of $\xi_1(t)$ and $\xi_2(t)$; that is,

$$\xi_1(t + T) = a_{11}\xi_1(t) + a_{12}\xi_2(t) \quad (3.24)$$

$$\xi_2(t + T) = a_{21}\xi_1(t) + a_{22}\xi_2(t) \quad (3.25)$$

Here, the a_{ij} are constants that can be determined by calculating two linearly independent solutions $\xi_1(t)$ and $\xi_2(t)$. Two linearly independent solutions of equation (3.23) were calculated for $t = [0, T]$ using the initial conditions

$$\xi_1(0) = 1, \quad \dot{\xi}_1(0) = 0 \quad (3.26)$$

$$\xi_2(0) = 0, \quad \dot{\xi}_2(0) = 1 \quad (3.27)$$

Hence, the a_{ij} are the elements of the so-called Monodromy matrix

$$\mathbf{A} = \begin{bmatrix} \xi_1(T) & \dot{\xi}_1(T) \\ \xi_2(T) & \dot{\xi}_2(T) \end{bmatrix} \quad (3.28)$$

The behavior of $\xi(t)$ and hence the stability of $\eta(t)$ depends on the eigenvalues (Floquet multipliers) λ_1 and λ_2 of \mathbf{A} . If both Floquet multipliers lie inside the unit circle, then $\xi(t) \rightarrow 0$ as $t \rightarrow \infty$ and hence $\eta(t)$ is stable. If one of the Floquet multipliers lies outside the unit circle, then $\eta(t)$ is unstable. The type of

instability that occurs as a control parameter is varied depends on how the Floquet multiplier leaves the unit circle. For the single-degree-of-freedom studied, λ can either leave the unit circle along the real axis through $+1$ or -1 . If λ leaves the unit circle through $+1$ a saddle-node bifurcation occurs. If λ leaves the unit circle through -1 a period-doubling bifurcation occurs.

Figure 9 shows a comparison of the bifurcation diagram generated by applying Floquet theory to the analytically calculated periodic solutions and the numerical results. It is obvious that the analytical solution predicts the saddle-node bifurcation very accurately. The analytical solution does not predict the onset of period-doubling bifurcations as accurately as the saddle-node; it, nevertheless, predicts the bifurcation to within a 9% error.

3.4.2 Method of Strained Parameters

Next we use the method of strained parameters (Nayfeh, 1981) to predict the onset of period-doubling bifurcations. To this end, we substitute equation (3.16) into equation (3.23) and obtain to second order

$$\ddot{\xi} + 2\mu\dot{\xi} + K^*\xi = \chi\xi \cos \Phi + \Lambda\xi \cos 2\Phi \quad (3.29a)$$

$$\Phi = \Omega t + \beta + \phi_e \quad (3.29b)$$

where K^* , χ , and Λ are defined in Appendix C. We introduce a small dimensionless parameter ε as a bookkeeping device and order the damping and parametric term at $O(\varepsilon)$, and rewrite equation (3.29a) as

$$\ddot{\xi} + 2\varepsilon\mu\dot{\xi} + K^*\xi = \varepsilon\chi\xi \cos \Phi + \varepsilon\Lambda\xi \cos 2\Phi \quad (3.30)$$

We seek a uniform expansion of the solutions of equation (3.30) in the form

$$\xi(t; \varepsilon) = \varepsilon\xi_1(t) + \varepsilon^2\xi_2(t) + \dots \quad (3.31)$$

$$K^* = \frac{1}{4}\Omega^2 + \varepsilon\delta_1 + \varepsilon^2\delta_2 + \dots \quad (3.32)$$

According to this method, we determine δ_1 and δ_2 such that the resulting expansion is periodic. Thus, equation (3.32) defines the transition curves separating stability from instability (i.e., transition curve for period-doubling bifurcation).

Substituting equations (3.31) and (3.32) into equation (3.30) and equating the coefficients of equal powers of ε on both sides, we have

$$\ddot{\xi}_0 + \frac{1}{4}\Omega^2\xi_0 = 0 \quad (3.33)$$

$$\ddot{\xi}_1 + \frac{1}{4}\Omega^2\xi_1 = -2\mu\dot{\xi}_0 - \delta_1\xi_0 + \chi\xi_0 \cos \Phi + \Lambda\xi_0 \cos 2\Phi \quad (3.34)$$

$$\ddot{\xi}_2 + \frac{1}{4}\Omega^2\xi_2 = -2\mu\dot{\xi}_1 - \delta_1\xi_1 - \delta_2\xi_2 + \chi\xi_1 \cos \Phi + \Lambda\xi_1 \cos 2\Phi \quad (3.35)$$

$$\xi_0 = a \cos \frac{1}{2} \Phi + b \sin \frac{1}{2} \Phi \quad (3.36)$$

where a and b are constants.

Substituting equation (3.36) into equation (3.34), we obtain

$$\begin{aligned} \ddot{\xi}_1 + \frac{1}{4} \Omega^2 \xi_1 = & \left[\left(\frac{1}{2} \chi - \delta_1 \right) a - \mu \Omega b \right] \cos \frac{1}{2} \Phi \\ & + \left[\mu \Omega a - \left(\frac{1}{2} \chi + \delta_1 \right) b \right] \sin \frac{1}{2} \Phi \\ & + \frac{1}{2} (\chi + \Lambda) a \cos \frac{3}{2} \Phi + \frac{1}{2} (\chi - \Lambda) b \sin \frac{3}{2} \Phi + \dots \end{aligned} \quad (3.37)$$

Eliminating the terms that produce secular terms in equation (3.37) requires that

$$\left(\frac{1}{2} \chi - \delta_1 \right) a - \mu \Omega b = 0 \quad (3.38)$$

$$\mu \Omega a - \left(\frac{1}{2} \chi + \delta_1 \right) b = 0 \quad (3.39)$$

For a nontrivial solution to exist

$$\delta_1^2 = \frac{1}{4} \chi^2 - \mu^2 \Omega^2 \quad (3.40)$$

Using equations (3.38) and (3.39), we express the solution of (3.37) in the form

$$\begin{aligned} \xi_1 = & D \cos \frac{1}{2} \Phi + E \sin \frac{1}{2} \Phi \\ & - \frac{(\chi + \Lambda)a}{4\Omega^2} \cos \frac{3}{2} \Phi - \frac{(\chi - \Lambda)b}{4\Omega^2} \sin \frac{3}{2} \Phi + \dots \end{aligned} \quad (3.41)$$

where D and E are constants. Substituting equations (3.36) and (3.41) into equation (3.35) and eliminating the secular terms, we have

$$\left(\frac{1}{2} \chi - \delta_1 \right) D - \mu \Omega E = \left[\delta_2 + \frac{(\chi + \Lambda)\Lambda}{8\Omega^2} \right] a \quad (3.42)$$

$$\mu \Omega D - \frac{1}{2} (\chi + \delta_1) E = \left[\delta_2 + \frac{(\chi - \Lambda)\Lambda}{8\Omega^2} \right] b \quad (3.43)$$

Because the homogeneous equations (3.42) and (3.43) have a nontrivial solution, the inhomogeneous equations have a solution if and only if a consistency (solvability) condition is satisfied; that is,

$$\delta_2 = - \frac{\chi^2 + 4\Lambda\delta_1 + \Lambda^2}{8\Omega^2} \quad (3.44)$$

Hence, the transition curves determining the period-doubling bifurcation are given by

$$K^* = \frac{1}{4} \Omega^2 \pm \varepsilon \left(\frac{1}{4} \chi^2 - \mu^2 \Omega^2 \right)^{1/2} - \varepsilon^2 \frac{\chi^2 \pm 4 \left(\frac{1}{4} \chi^2 - \mu^2 \Omega^2 \right)^{1/2} \Lambda + \Lambda^2}{8\Omega^2} + \dots \quad (3.45)$$

Equation (3.45) predicts the onset of period-doubling bifurcations to within a 10% error. The accuracy would probably improve if more terms were kept in

equations (3.30)-(3.32), however, the algebra would become much more involved.

Harmonic Balance

The third method used to determine the period-doubling bifurcations is the method of harmonic balance. Using the analytical solution as a guide in choosing the form of the solution of equation (3.29a), we assume a solution of the form

$$\eta = a \cos \frac{1}{2} \Phi + b \sin \frac{1}{2} \Phi + c \cos \frac{3}{2} \Phi + d \sin \frac{3}{2} \Phi \quad (3.46)$$

Substituting equation (3.46) into equation (3.29a), equating the coefficients of the different harmonics, and setting the determinant of the resulting coefficient matrix equal to zero, we have

$$81\Omega^8 + \gamma_1\Omega^6 + \gamma_2\Omega^4 + \gamma_3\Omega^2 + \gamma_4 = 0 \quad (3.47)$$

where the γ_i are defined in Appendix C. From equations (3.19) and (3.47) we obtained the curves shown in Figure 9. Again this method predicts the onset of saddle-node bifurcations very well, but it has difficulty in predicting the onset of period-doubling bifurcations.

3.4.4 Tangent Instability

To determine the tangent (saddle-node) instabilities we locate the points corresponding to the vertical tangents (infinite slopes) in the frequency-response curves given by equation (3.19). We begin by rewriting equation (3.19) as

$$4\mu^2\Omega^2 + (\sigma + 2\alpha_e a^2)^2 = \frac{g^2}{a^2} \quad (3.48)$$

Letting $p = a^2$, $x = \Omega^2$, and $\sigma = \omega_0^2 - \Omega^2$ we have

$$4\mu^2 xp + p(\omega_0^2 - x + 2\alpha_e p)^2 = g^2 \quad (3.49)$$

Taking the derivative of equation (3.49) with respect to x , we obtain

$$4\mu^2 x \frac{dp}{dx} + (\omega_0^2 - x + 2\alpha_e p)^2 \frac{dp}{dx} + 4\alpha_e p (\omega_0^2 - x + 2\alpha_e p) \frac{dp}{dx} + 4\mu^2 p - 2p(\omega_0^2 - x + 2\alpha_e p) = 0 \quad (3.50)$$

Setting the coefficient of $\frac{dp}{dx}$ equal to zero, we have

$$4\mu^2 x + (\omega_0^2 - x + 2\alpha_e p)^2 + 4p\alpha_e(\omega_0^2 - x + 2\alpha_e p) = 0 \quad (3.51)$$

It follows from equations (3.49) and (3.51) that

$$g^2 = 4p^2\alpha_e(\omega_0^2 - x + 2\alpha_e p) \quad (3.52)$$

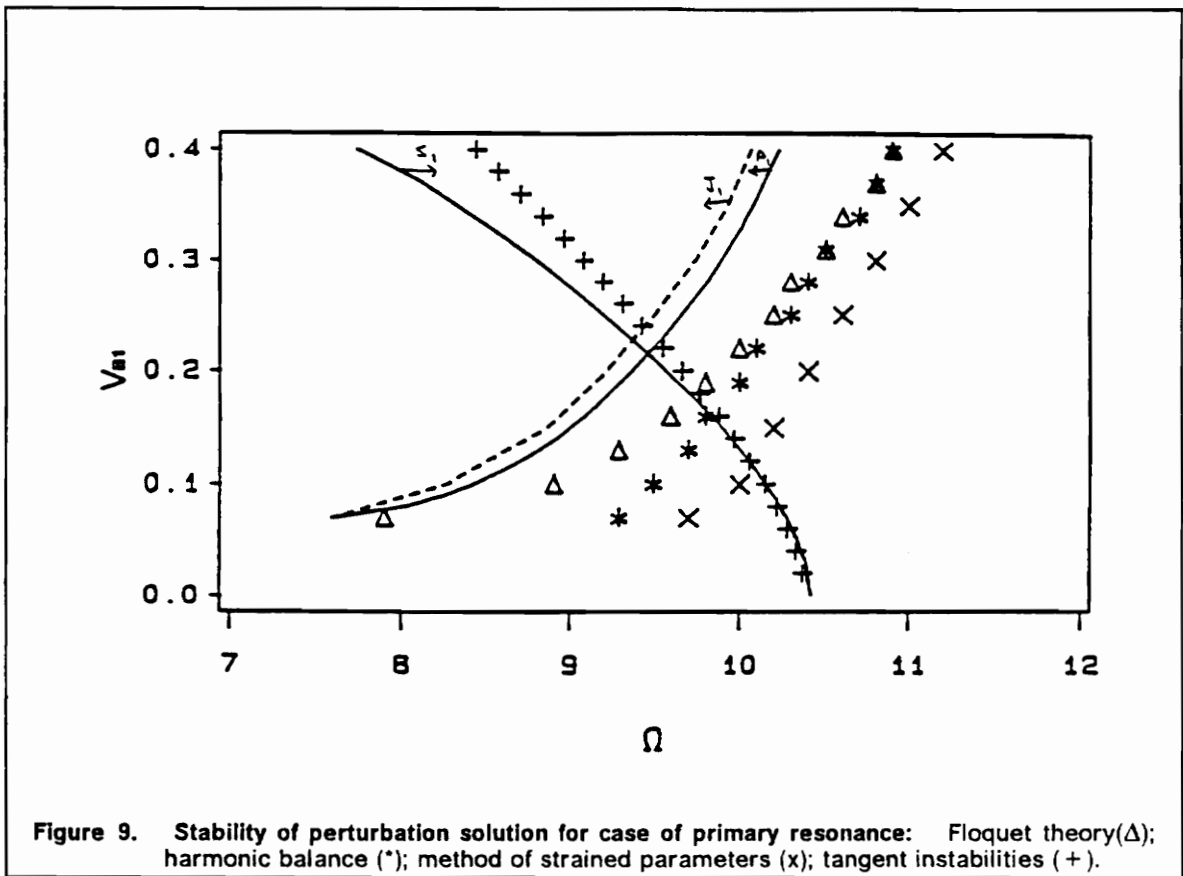
Next, we let

$$z = \omega_0^2 - x + 2\alpha_e p \quad (3.53)$$

Substituting equation (3.53) into equation (3.51) we obtain

$$3z^2 + 2z(\omega_0^2 + x) + 4\mu^2 x = 0 \quad (3.54)$$

To locate the tangent instability curve, we determine z from equation (3.54) for a specific value of Ω , then compute p from equation (3.53), and finally compute g from equation (3.52). The results obtained by using this technique are very accurate, as can be seen from Figure 9.



CHAPTER 4

Subharmonic Resonance

4.1 Introduction

In this chapter, we use numerical simulations and perturbation analyses to understand the behavior of the system near the subharmonic resonance of order one-half. Numerical simulations are used to show that the combined effect of a principal parametric resonance and a subharmonic resonance of order one-half leads to complicated dynamics. As the excitation frequency is varied, we demonstrate that the response undergoes a sequence of period-doubling bifurcations culminating in chaos, after which the solution becomes unbounded. Using numerical simulations alone to locate the regions of complex behavior requires a lot of time and effort. Thus it is of interest to develop approximate solutions that will reduce the time and effort. First, we

investigated the use of the first-order perturbation solution of Hamdan and Nayfeh (1989). We found that this expansion predicts fairly accurately the period-one motions and their bifurcations into period-two motions for small excitation amplitudes. However, as the excitation amplitude increases, we found that the first-order perturbation solution becomes less accurate. Therefore, we use the method of multiple scales to determine a second-order approximate solution that improves on the accuracy of the solution given by Hamdan and Nayfeh (1989), and whose loss of stability agrees fairly well with the onset of period-doubling bifurcations, which is a precursor to chaos and loss of synchronism.

4.2 Numerical Simulation

Equations (1.1)-(1.3) were simulated on the digital computer by using a fifth- and sixth-order Runge-Kutta algorithm. The parameters of the system are listed in Appendix D. We studied the effect of varying the excitation frequency Ω near the subharmonic resonance of order one-half; that is, $\Omega \approx 2\omega_0$. The effect of varying the excitation frequency Ω and the initial conditions is shown in Figure 10.

For Ω much larger than $2\omega_0$, the steady-state solution (attractor) is periodic having the period $2\pi/\Omega$. The phase portrait corresponds to a period-one limit cycle (Figure 10a). This can be verified by observing the corresponding FFT

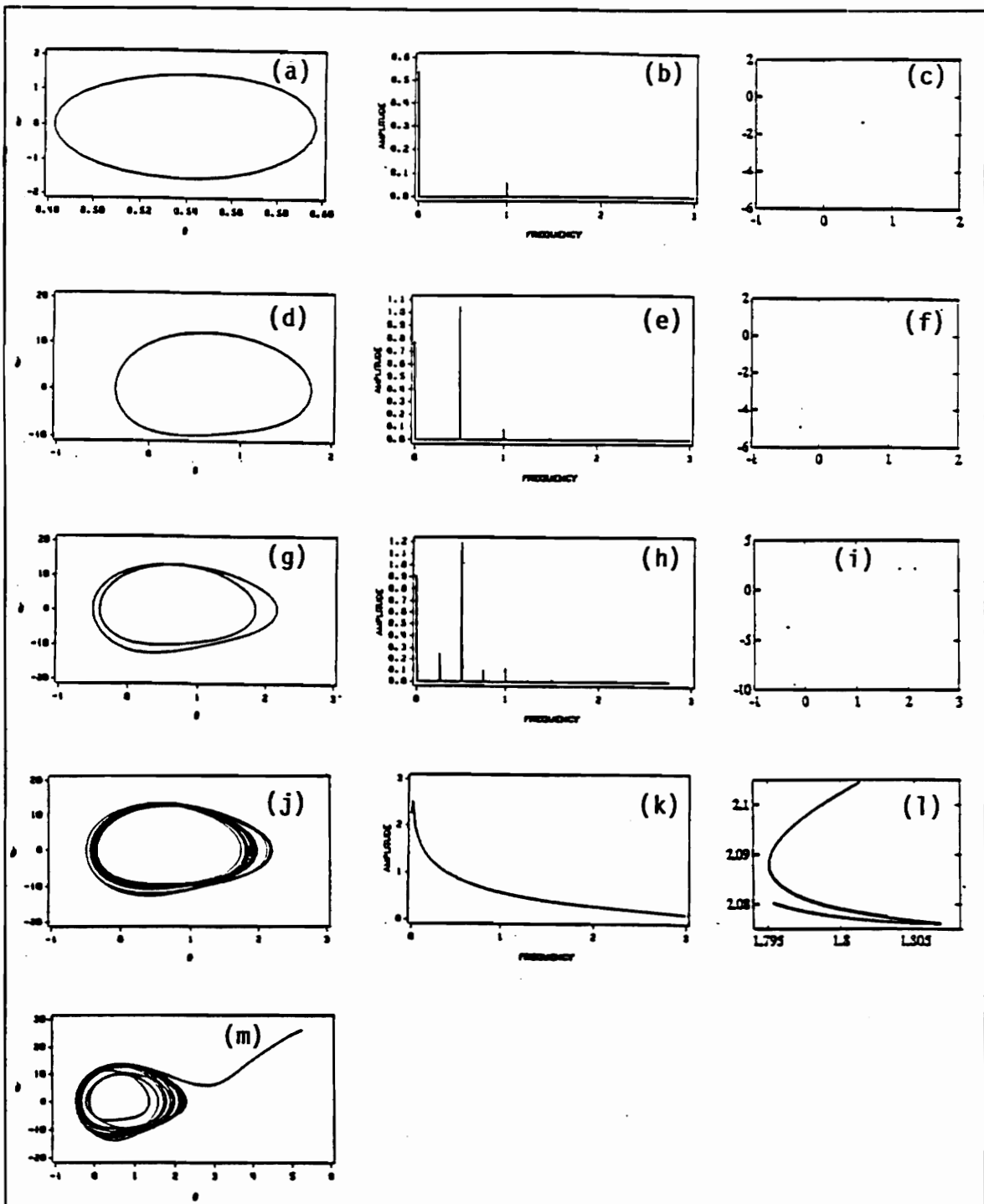


Figure 10. Numerical simulation for case of subharmonic resonance: (a)-(c) period-one $\Omega = 26.0$ rad/sec; (d)-(f) period-two $\Omega = 21.03$ rad/sec; (g)-(i) period-four $\Omega = 19.416$ rad/sec; (j)-(l) chaos $\Omega = 19.374$ rad/sec; (m) loss of synchronization $\Omega = 19.373$ rad/sec.

(Figure 10b) and Poincaré map (Figure 10c), where the FFT consists of frequency components at Ω and its harmonics and the Poincaré map contains only one point. As Ω is decreased, the period-one orbit deforms until Ω reaches the threshold value 24.155 rad/sec, where the period-one attractor loses its stability and gives way to a period-two attractor (Figure 10d) with the period $4\pi/\Omega$. The FFT (Figure 10e) and Poincaré map (Figure 10f) verify the occurrence of a period-doubling bifurcation. The FFT has new frequency components at $\frac{1}{2}\Omega$, $\frac{3}{2}\Omega$, $\frac{5}{2}\Omega$, ... and their harmonics and the Poincaré map contains two points. As Ω is decreased further the period-two orbit deforms until it goes through a period-doubling bifurcation at $\Omega = 19.65$ rad/sec. The phase portrait shows an attractor consisting of two loops as shown in Figure 10g; the period of this attractor is $8\pi/\Omega$. These period-doubling bifurcations continue as Ω is decreased further and eventually the solution becomes chaotic at $\Omega = 19.374$ rad/sec (Figure 10j). The FFT of the chaotic attractor (Figure 10k) has a broadband power spectrum and the Poincaré map (Figure 10l) shows a strange attractor. The corresponding Liapunov exponents are 1.4437, 0.0, -7.452 and the Liapunov dimension $D_L = 2.19$. As Ω is decreased even further ($\Omega = 19.373$ rad/sec), the sequence of bifurcations culminates in an unbounded motion (Figure 10m) (i.e., loss of synchronism).

As in Chapter 3 we study the behavior of the solutions of equations (1.1)-(1.3) in the two parameter space corresponding to the frequency Ω and amplitude V_{B_1} of the external excitation (Figure 11). The region on the left side of the bifurcation diagram corresponds to the region studied in Chapter 3. If a

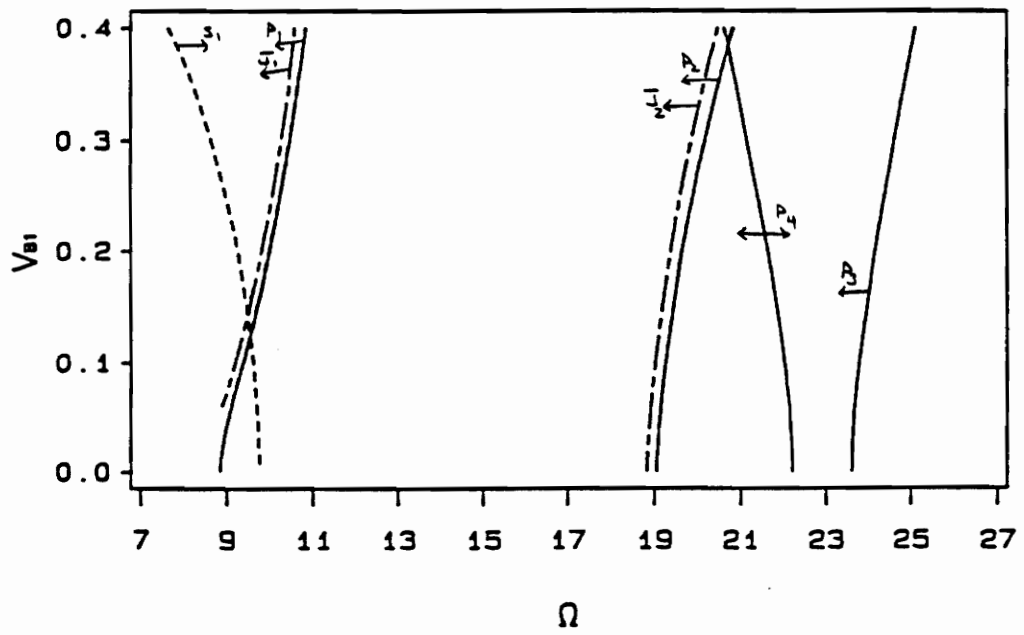
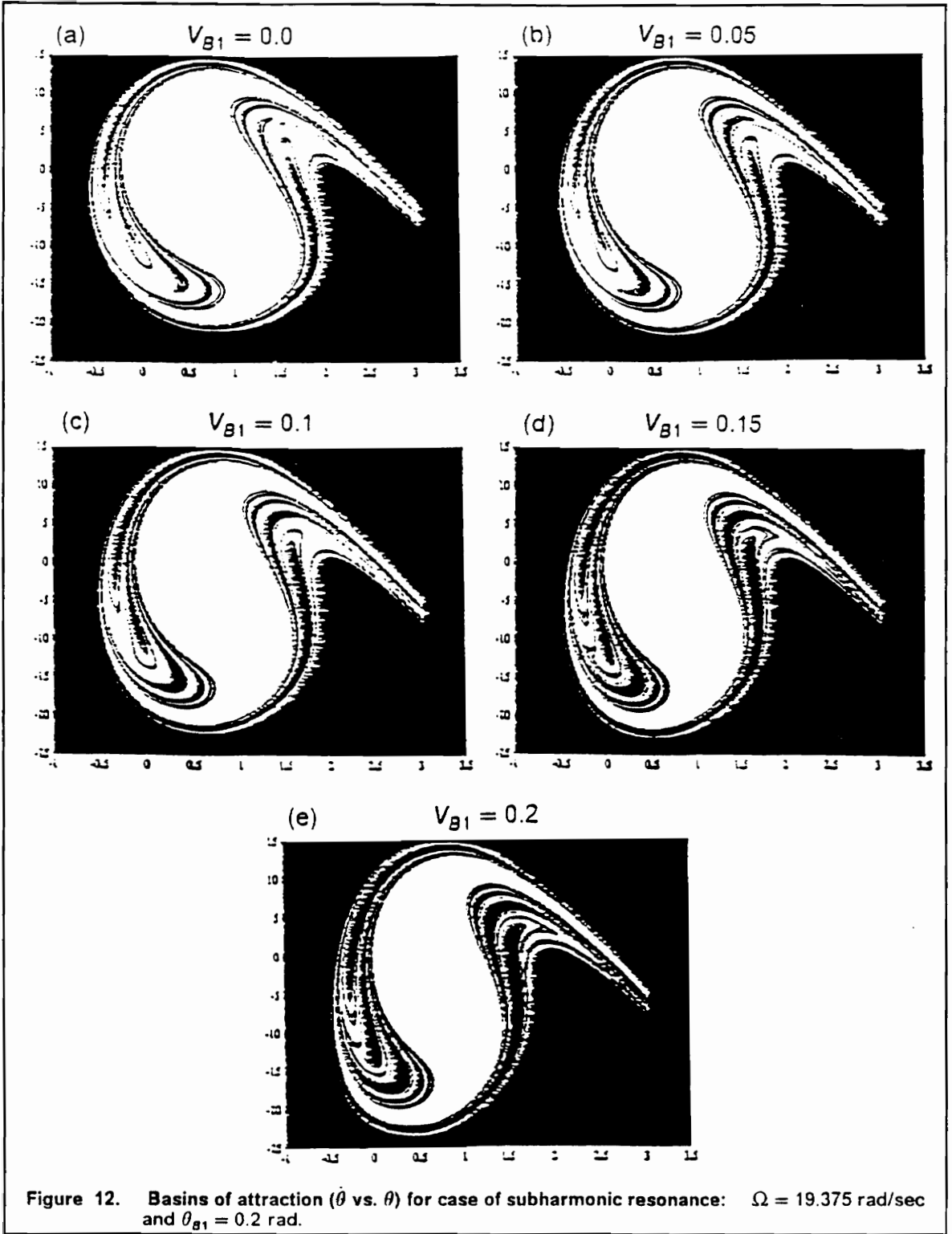


Figure 11. Bifurcation diagram for case of subharmonic resonance

parameter is varied across S_1 , the small attractor loses its stability through a saddle-node bifurcation. The system response will either go unbounded for values of $V_{B1} > C_1$ or jump to the large attractor for values of $V_{B1} < C_1$. The large attractor will go through a sequence of period-doubling bifurcations if any parameters are varied across P_1 . If a parameter is varied across J_1 the chaotic attractor either goes unbounded ($V_{B1} > C_1$) or jumps to the small attractor ($V_{B1} < C_1$). The large attractor loses its stability in the region of the subharmonic resonance $\Omega = 2.0$ rad/sec. The primary resonant response is unstable in the region between P_3 and P_4 . When P_3 is crossed from left to right the attractor goes through a period-doubling bifurcation and jumps to the subharmonic response. If P_4 is crossed from left to right the subharmonic response loses its stability and jumps to the primary resonant response.

The primary resonant response loses its stability through a period-doubling bifurcation for parameter variations across P_4 (right to left), giving rise to the subharmonic response. The subharmonic response goes through a sequence of period-doubling bifurcations leading to chaos when P_2 is crossed from right to left. The chaotic attractor loses its stability and jumps to the primary resonant response for values of $V_{B1} < C_2$ and goes unbounded for values of $V_{B1} > C_2$.

Of major importance is the ability to predict regions of bounded and unbounded motions. Hence, we studied various basins of attraction for different values of V_{B1} and θ_{B1} . We studied the region $-1 \leq \theta \leq 3.5$ and



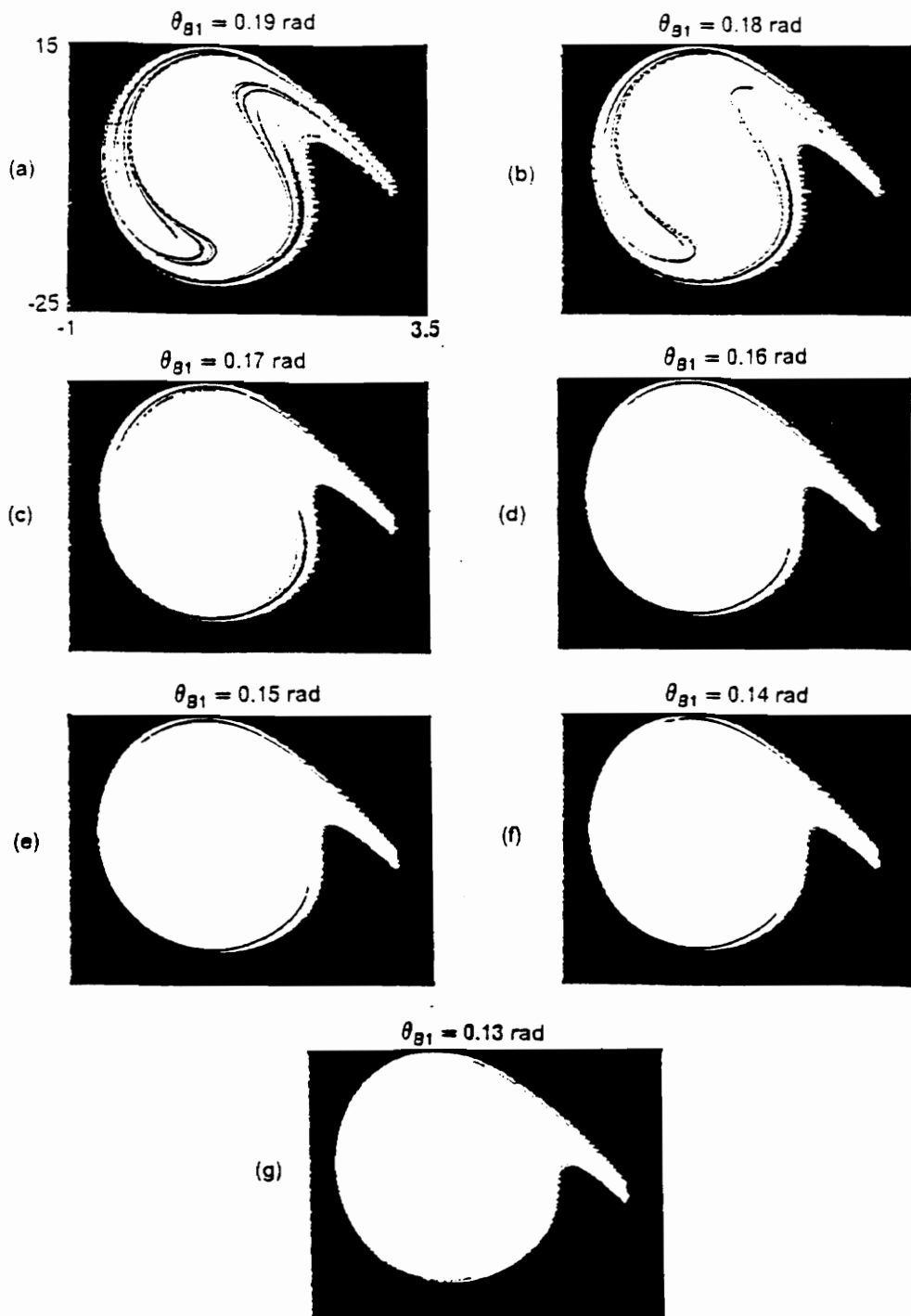


Figure 13. Basins of attraction (θ vs. θ) for case of subharmonic resonance: $\Omega = 19.375$ rad/sec and $V_{B1} = 0.0$ rad.

$-25 \leq \theta \leq 15$ with a grid of 400x450 initial conditions. Figure 12 shows a series of metamorphoses that the system undergoes as V_{B1} is varied for $\Omega = 19.375$ rad/sec and $\theta_{B1} = 0.2$ rad. At $V_{B1} = 0.2$ (Figure 12a) the basin of attraction seems fractal. The fractal nature of the basin indicates the sensitivity to initial conditions present at this voltage. As V_{B1} is decreased the fingers begin to subside; however, even for $V_{B1} = 0.0$ the basin of attraction is still corrupted by regions of unbounded motions, this is due to the effect of θ_{B1} .

Figure 13 shows the metamorphoses that the basin of attraction undergoes as θ_{B1} is varied with $V_{B1} = 0.0$. As θ_{B1} is decreased, the fingers of unbounded motions decrease and eventually disappear at $\theta_{B1} = 0.13$ (Figure 13f). Values of $\theta_{B1} < 0.13$ correspond to smooth basin boundaries. Eventually, at $\theta_{B1} = 0.0$ the system will have basin boundaries defined by the separatrices of the free damped oscillations of the system (Figure 2b).

4.3 Perturbation Analysis

To predict the onset of the period-doubling bifurcations, which are precursors to chaos and loss of synchronism, we use the method of multiple scales (Nayfeh, 1973,1981) to determine a second-order approximate expression for the period-two solutions for the case of $\Omega \approx 2\omega_0$. We demonstrate how a

second-order analytical approximate solution can be used to predict the onset of complex dynamics and instability.

Hamdan and Nayfeh (1989) used a first-order expansion where the nonlinearities and damping terms were ordered to counter the effect of resonances. Thus, the nonlinear, damping, and excitation terms were ordered so that their effects occur at the same order. Their solution becomes less accurate as the excitation amplitude increases because of its inability to account for the frequency shift caused by the external excitation. In this chapter, we extend their analysis to second order, thereby accounting for the frequency shift due to the external excitation. To accomplish this, we introduce a small dimensionless parameter ε that is used as a bookkeeping device and will be set unity in the final analysis. If $\eta = 0(\varepsilon)$, then we let $\omega_R D/2H = 0(\varepsilon)$, $F_1 = 0(\varepsilon)$, $G = 0(\varepsilon)$, and we assume that $V_{B1} = 0(\varepsilon)$ and $\theta_{B1} = 0(\varepsilon)$. Quantitatively, this implies that

$$F_1 = \varepsilon f_1, F_2 = \varepsilon F_2, F_3 = \varepsilon f_3, \text{ and } G = \varepsilon g$$

With these orderings equation (1.6) can be rewritten as

$$\begin{aligned} \ddot{\eta} + 2\varepsilon\mu\dot{\eta} + \omega_0^2\eta &= \alpha_2\eta^2 + \alpha_3\eta^3 + \varepsilon f_1\eta \cos(\Omega t + \phi_v) \\ &+ \varepsilon f_2\eta^2 \cos(\Omega t + \phi_v) + \varepsilon f_3\eta^3 \cos(\Omega t + \phi_v) \\ &+ \varepsilon g \cos(\Omega t + \phi_e) \end{aligned} \quad (4.1)$$

where $\mu = \omega_R D/4H$.

We seek a second-order uniform solution of equation (4.1) in the form

$$\begin{aligned} \eta(t; \varepsilon) = & \varepsilon\eta_1(T_0, T_1, T_2) + \varepsilon^2\eta_2(T_0, T_1, T_2) \\ & + \varepsilon^3\eta_3(T_0, T_1, T_2) + \dots \end{aligned} \quad (4.2)$$

where $T_0 = t$ is a fast scale, characterizing motions occurring at the frequencies Ω and ω_0 , and $T_1 = \varepsilon t$ and $T_2 = \varepsilon^2 t$ are slow scales, describing the modulation of the amplitude and phase with damping, nonlinearities, and resonances. In terms of these time scales, the time derivatives become

$$\frac{d}{dt} = D_0 + \varepsilon D_1 + \varepsilon^2 D_2 + \dots \quad (4.3)$$

$$\frac{d^2}{dt^2} = D_0^2 + 2\varepsilon D_0 D_1 + \varepsilon^2 (2D_0 D_2 + D_1^2) + \dots \quad (4.4)$$

where $D_n = \partial/\partial T_n$. To express the nearness of Ω to $2\omega_0$, we introduce the detuning parameter σ according to

$$\omega_0^2 = \frac{1}{4} \Omega^2 + \varepsilon\sigma \quad (4.5)$$

This detuning is different from that used in Hamdan and Nayfeh (1989). It has the advantage of allowing larger deviations of Ω from $2\omega_0$. Substituting equations (4.2)-(4.5) into equation (4.1) and equating coefficients of like powers of ε , we obtain

$$D_0^2 \eta_1 + \frac{1}{4} \Omega^2 \eta_1 = g \cos(\Omega t + \phi_e) \quad (4.6)$$

$$D_0^2 \eta_2 + \frac{1}{4} \Omega^2 \eta_2 = -2\mu D_0 \eta_1 - 2D_0 D_1 \eta_1 - \sigma \eta_1 + \alpha_2 \eta_1^2 + f_1 \eta_1 \cos(\Omega T_0 + \phi_v) \quad (4.7)$$

$$D_0^2 \eta_3 + \frac{1}{4} \Omega^2 \eta_3 = -\sigma \eta_2 - 2D_0 D_1 \eta_2 - (D_1^2 + 2D_0 D_2) \eta_1 - 2\mu(D_1 \eta_1 + D_0 \eta_2) + 2\alpha_2 \eta_1 \eta_2 + \alpha_3 \eta_1^3 + f_1 \eta_2 \cos(\Omega T_0 + \phi_v) + f_2 \eta_1^2 \cos(\Omega T_0 + \phi_v) \quad (4.8)$$

The solution of equation (4.6) can be expressed in either the form

$$\eta_1 = a(T_0, T_1, T_2) \cos\left[\frac{1}{2} \Omega T_0 + \beta(T_0, T_1, T_2)\right] + 2\Lambda \cos(\Omega T_0 + \phi_e) \quad (4.9)$$

or the form

$$\eta_1 = A(T_1, T_2) e^{\frac{1}{2} i \Omega T_0} + \bar{A}(T_1, T_2) e^{-\frac{1}{2} i \Omega T_0} + \Lambda e^{i \Omega T_0} + \bar{\Lambda} e^{-i \Omega T_0} \quad (4.10)$$

where \bar{A} is the complex conjugate of A and

$$\Lambda = -\frac{2g}{3\Omega^2} e^{i\phi_e} \quad (4.11a)$$

Comparing equations (4.9) and (4.10) shows that

$$A = \frac{1}{2} a e^{i\beta} \quad (4.11b)$$

Substituting equation (4.10) into equation (4.7) leads to

$$\begin{aligned}
 D_0^2 \eta_2 + \frac{1}{4} \Omega^2 \eta_2 = & \left[-i\Omega(D_1 A + \mu A) - \sigma A + 2\alpha_2 \Lambda \bar{A} \right. \\
 & + \left. \frac{1}{2} f_1 \bar{A} e^{i\phi_v} \right] e^{\frac{1}{2} i\Omega T_0} + \left[-2i\mu\Omega\Lambda - \sigma\Lambda + \alpha_2 A^2 \right] e^{i\Omega T_0} \\
 & + \left[2\alpha_2 A\Lambda + \frac{1}{2} A f_1 e^{i\phi_v} \right] e^{\frac{3}{2} i\Omega T_0} + \left[\alpha_2 (A\bar{A} + \Lambda\bar{\Lambda}) + \frac{1}{2} \bar{\Lambda} f_1 e^{i\phi_v} \right] \\
 & + \left[\alpha_2 \Lambda^2 + \frac{1}{2} f_1 \Lambda e^{i\phi_v} \right] e^{2i\Omega T_0} + cc
 \end{aligned} \tag{4.12}$$

where cc stands for the complex conjugate of the preceding terms. Eliminating the secular terms (terms that render the expansion nonuniform for large t) in equation (4.12), we have

$$-i\Omega D_1 A - i\Omega \mu A - \sigma A + \bar{A} \Gamma e^{i\phi_{ee}} = 0 \tag{4.13}$$

where

$$\Gamma e^{i\phi_{ee}} = 2\alpha_2 \Lambda + \frac{1}{2} f_1 e^{i\phi_v} \tag{4.14}$$

Hence, the solution of equation (4.12) can be written as

$$\begin{aligned}
 \eta_2 = & -\frac{4}{3\Omega^2} \left[\alpha_2 A^2 - (2i\mu\Omega + \sigma)\Lambda \right] e^{i\Omega T_0} - \frac{A}{2\Omega^2} \Gamma e^{i\left(\frac{3}{2}\Omega T_0 + \phi_{ee}\right)} \\
 & + \frac{4}{\Omega^2} \left[\alpha_2 (A\bar{A} + \Lambda\bar{\Lambda}) + \frac{1}{2} f_1 \bar{\Lambda} e^{i\phi_v} \right] \\
 & - \frac{4}{15\Omega^2} \left[\alpha_2 \Lambda^2 + \frac{1}{2} f_1 \Lambda e^{i\phi_v} \right] e^{2i\Omega T_0} + cc
 \end{aligned} \tag{4.15}$$

Substituting equations (4.10) and (4.15) into equation (4.8) yields

$$\begin{aligned}
D_0^2 \eta_3 + \frac{1}{4} \Omega^2 \eta_3 = & -i\Omega D_2 A - D_1^2 A - 2\mu D_1 A \\
& - \frac{8\alpha_2}{3\Omega^2} \left[-(2i\mu\Omega + \sigma)\Lambda\bar{A} + \alpha_2 A^2 \bar{A} \right] - \frac{\alpha_2 A \bar{\Lambda}}{\Omega^2} \Gamma e^{i\phi_{ee}} \\
& + \frac{8\alpha_2}{\Omega^2} \left[2\alpha_2 A^2 \bar{A} + 2\alpha_2 A \Lambda \bar{\Lambda} + \frac{1}{2} f_1 A (\bar{\Lambda} e^{i\phi_\nu} + \Lambda e^{-i\phi_\nu}) \right] \\
& + 6\alpha_3 A \Lambda \bar{\Lambda} + 3\alpha_3 A^2 \bar{A} - \frac{A f_1 \Gamma}{4\Omega^2} e^{i(\phi_{ee} - \phi_\nu)} \\
& + f_2 A (\bar{\Lambda} e^{i\phi_\nu} + \Lambda e^{-i\phi_\nu}) + NST + cc
\end{aligned} \tag{4.16}$$

It follows from equation (4.13) that

$$D_1 \bar{A} = -\left(\mu + \frac{i\sigma}{\Omega}\right) \bar{A} + \frac{i}{\Omega} A \Gamma e^{i\phi_{ee}} \tag{4.17}$$

and

$$D_1^2 A = \left[\mu^2 - \frac{2i\mu\sigma}{\Omega} + \frac{\Gamma^2 - \sigma^2}{\Omega^2} \right] A + \frac{2i\mu}{\Omega} \bar{A} \Gamma e^{i\phi_{ee}} \tag{4.18}$$

Eliminating the secular terms from equation (4.16) and using equations (4.13)

and (4.18), we obtain

$$\begin{aligned}
& -i\Omega D_2 A + \left[\mu^2 - \frac{\Gamma^2 - \sigma^2}{\Omega^2} - \frac{\alpha_2 \bar{\Lambda} \Gamma}{\Omega^2} e^{i\phi_{ee}} + \left(6\alpha_3 + \frac{16\alpha_2^2}{\Omega^2} \right) \Lambda \bar{\Lambda} \right. \\
& \left. + (\bar{\Lambda} e^{i\phi_\nu} + \Lambda e^{-i\phi_\nu}) \left(\frac{4\alpha_2 f_1}{\Omega^2} + f_2 \right) - \frac{\Gamma f_1}{4\Omega^2} e^{i(\phi_{ee} - \phi_\nu)} \right] A \\
& + \left(3\alpha_3 + \frac{40\alpha_2^2}{3\Omega^2} \right) A^2 \bar{A} + \frac{8\alpha_2}{3\Omega^2} (2i\mu\Omega + \sigma) \Lambda \bar{A} = 0
\end{aligned} \tag{4.19}$$

Using the method of reconstitution (Nayfeh, 1985), we form the derivative of A with respect to t by substituting equations (4.13) and (4.19) into equation (4.3), putting $\varepsilon = 1$, and obtaining

$$i\Omega(\dot{A} + \mu_e A) + \sigma_e A - 4\alpha_e A^2 \bar{A} - \hat{\Gamma} e^{i\hat{\phi}_e} = 0 \quad (4.20)$$

where the dot indicates the derivative with respect to t ,

$$\mu_e = \mu - \frac{2\alpha_2 g \Gamma}{3\Omega^5} \sin(\phi_{ee} - \phi_e) + \frac{\Gamma f_1}{4\Omega^3} \sin(\phi_{ee} - \phi_v), \quad (4.21)$$

$$\begin{aligned} \sigma_e = & \sigma - \mu^2 + \frac{\Gamma^2 - \sigma^2}{\Omega^2} - \left(\frac{2g}{3\Omega^2} \right)^2 (6\alpha_3 + \frac{16\alpha_2^2}{\Omega^2}) \\ & + \frac{4g}{3\Omega^2} (f_2 + \frac{4\alpha_2 f_1}{\Omega^2}) \cos(\phi_v - \phi_e) \\ & - \frac{2\alpha_2 g \Gamma}{3\Omega^4} \cos(\phi_{ee} - \phi_e) + \frac{\Gamma f_1}{4\Omega^2} \cos(\phi_{ee} - \phi_v), \end{aligned} \quad (4.22)$$

$$\alpha_e = \frac{10\alpha_2^2}{3\Omega^2} + \frac{3}{4} \alpha_3, \quad (4.23)$$

and

$$\hat{\Gamma} e^{i\hat{\phi}_e} = \Gamma e^{i\phi_{ee}} - \frac{16\alpha_2 g}{9\Omega^4} (2i\mu\Omega + \sigma) e^{i\phi_e} \quad (4.24)$$

Expressing A in the polar form (4.11b) and separating real and imaginary parts in equation (4.20), we obtain

$$\Omega(\dot{a} + \mu_e a) - a\hat{\Gamma} \sin \gamma = 0 \quad (4.25)$$

$$-\Omega a\dot{\beta} + \sigma_e a - \alpha_e a^3 - a\hat{\Gamma} \cos \gamma = 0 \quad (4.26)$$

where

$$\gamma = \hat{\phi}_e - 2\beta \quad (4.27)$$

Therefore, to the second approximation

$$\begin{aligned} \eta = & a \cos \left[\frac{1}{2} (\Omega t + \hat{\phi}_e - \beta) \right] - \frac{4g}{3\Omega^2} \cos(\Omega t + \phi_e) \\ & + \frac{32\mu g}{9\Omega^3} \sin(\Omega t + \phi_e) - \frac{16\sigma g}{9\Omega^4} \cos(\Omega t + \phi_e) \\ & - \frac{2a^2\alpha_2}{3\Omega^2} \cos(\Omega t + \hat{\phi}_e - \gamma) - \frac{32\alpha_2 g^2}{135\Omega^6} \cos[2(\Omega t + \phi_e)] \\ & - \frac{af_1}{4\Omega^2} \cos \left[\frac{3}{2} \Omega t + \phi_v + \frac{1}{2} (\hat{\phi}_e - \gamma) \right] + \frac{2\alpha_2}{\Omega^2} \left(a^2 + \frac{16g^2}{9\Omega^4} \right) \\ & - \frac{8f_1 g}{3\Omega^4} \cos(\phi_v - \phi_e) + \frac{2\alpha_2 a g}{3\Omega^4} \cos \left[\frac{3}{2} \Omega t + \phi_e + \frac{1}{2} (\hat{\phi}_e - \gamma) \right] \\ & + \frac{8f_1 g}{45\Omega^4} \cos(2\Omega t + \phi_e + \phi_v) + \dots \end{aligned} \quad (4.28)$$

Consequently,

$$\begin{aligned}
\Delta\theta = & \theta_{B1} \cos(\Omega t + \phi_\theta) + a \cos\left[\frac{1}{2}(\Omega t + \hat{\phi}_e - \beta)\right] - \frac{4g}{3\Omega^2} \cos(\Omega t + \phi_e) \\
& + \frac{32\mu g}{9\Omega^3} \sin(\Omega t + \phi_e) - \frac{16\sigma g}{9\Omega^4} \cos(\Omega t + \phi_e) - \frac{2a^2\alpha_2}{3\Omega^2} \cos(\Omega t + \hat{\phi}_e - \gamma) \\
& + \frac{2\alpha_2 a g}{3\Omega^4} \cos\left[\frac{3}{2}\Omega t + \phi_e + \frac{1}{2}(\hat{\phi}_e - \gamma)\right] \\
& - \frac{af_1}{4\Omega^2} \cos\left[\frac{3}{2}\Omega t + \phi_v + \frac{1}{2}(\hat{\phi}_e - \gamma)\right] + \frac{2\alpha_2}{\Omega^2} \left(a^2 + \frac{16g^2}{9\Omega^4}\right) \\
& + \frac{8f_1 g}{3\Omega^4} \cos(\phi_v - \phi_e) - \frac{32\alpha_2 g^2}{135\Omega^6} \cos[2(\Omega t + \phi_e)] \\
& + \frac{8f_1 g}{45\Omega^4} \cos(2\Omega t + \phi_e + \phi_v) + \dots
\end{aligned} \tag{4.29}$$

For the steady state, we have $\dot{a} = \dot{\beta} = 0$. Hence equations (4.25)-(4.27) become

$$\Omega\mu_e a - \hat{\Gamma} a \sin \gamma = 0 \tag{4.30}$$

$$\sigma_e a - \alpha_e a^3 + \hat{\Gamma} a \cos \gamma = 0 \tag{4.31}$$

It follows from equations (4.30) and (4.31) that the steady-state amplitude can be either trivial (i.e., $a = 0$) or nontrivial (i.e., $a \neq 0$). When $a = 0$ it follows from equations (1.4) and (4.29) that the variations in the rotor angle of the machine are given by

$$\begin{aligned}
\Delta\theta = & \theta_{B1} \cos(\Omega t + \phi_e) - \frac{4g}{3\Omega^2} \cos(\Omega t + \phi_e) + \frac{32\mu g}{9\Omega^2} \sin(\Omega t + \phi_e) \\
& - \frac{16\sigma g}{9\Omega^4} \cos(\Omega t + \phi_e) + \frac{32\alpha_2 g^2}{9\Omega^6} - \frac{8f_1 g}{3\Omega^4} \cos(\phi_v - \phi_e) \\
& + \frac{32\alpha_2 g^2}{135\Omega^6} \cos[2(\Omega t + \phi_e)] + \frac{8f_1 g}{45\Omega^4} \cos(2\Omega t + \phi_e + \phi_v)
\end{aligned} \tag{4.32}$$

When $a \neq 0$, one can eliminate γ from equations (4.30) and (4.31) to obtain the frequency-response equation

$$a^2 = \frac{1}{\alpha_e} \left[\sigma_e \pm \sqrt{\hat{\Gamma}^2 - \Omega^2 \mu_e^2} \right] \tag{4.33}$$

Equation (4.33) relates the amplitude of the response to the frequency of the excitation. The plot of a as a function of Ω is called the frequency-response curve (Figure 14).

4.3.1 Comparison of the Perturbation Solution with Numerical Simulations

To analyze the accuracy of our closed-form analytical solution, we compare it with numerical simulations of equations (1.1)-(1.3). For a given Ω , we calculate a from equation (4.33) and then calculate γ from equations (4.30) and (4.31). Substituting the values of a and γ into equations (4.28), we determine η and $\dot{\eta}$ from equations (3.20) and (3.21). A typical long-time history of the response

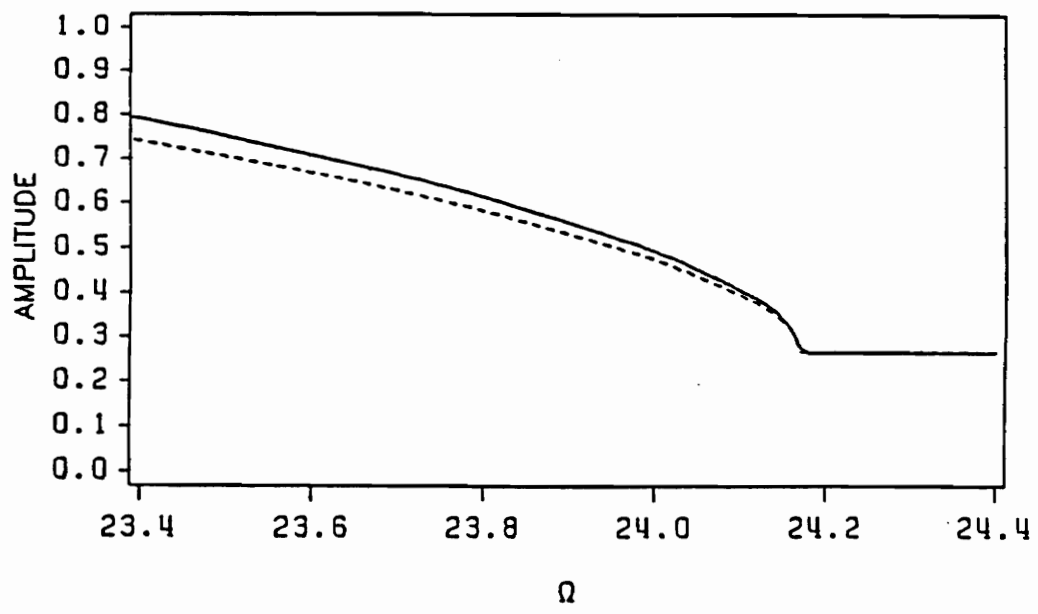
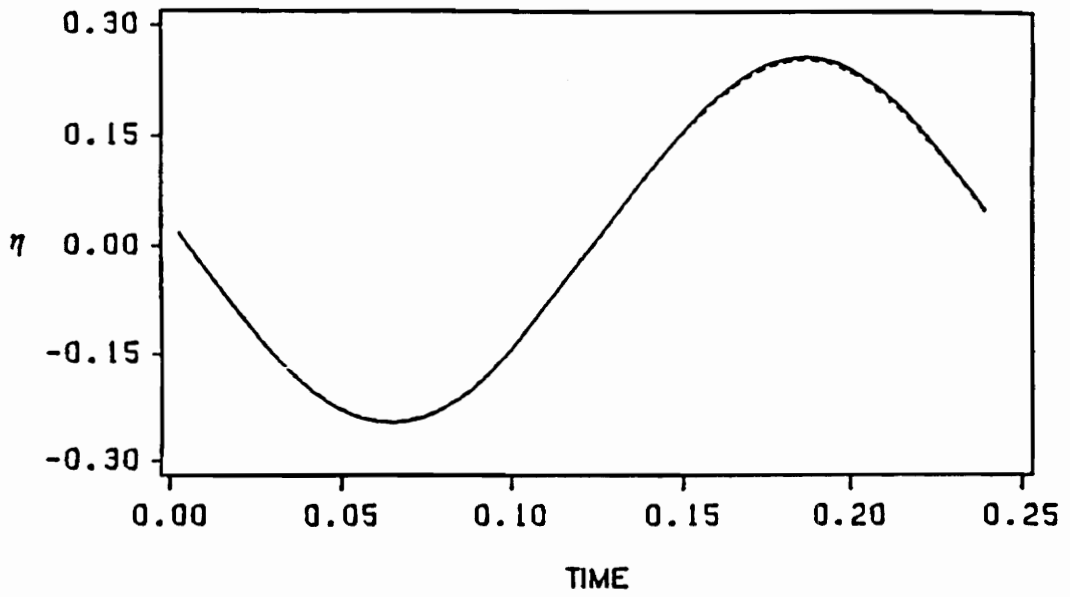


Figure 14. Frequency-response curve for case of subharmonic resonance: numerical simulation (---); perturbation solution (___)

(a)



(b)

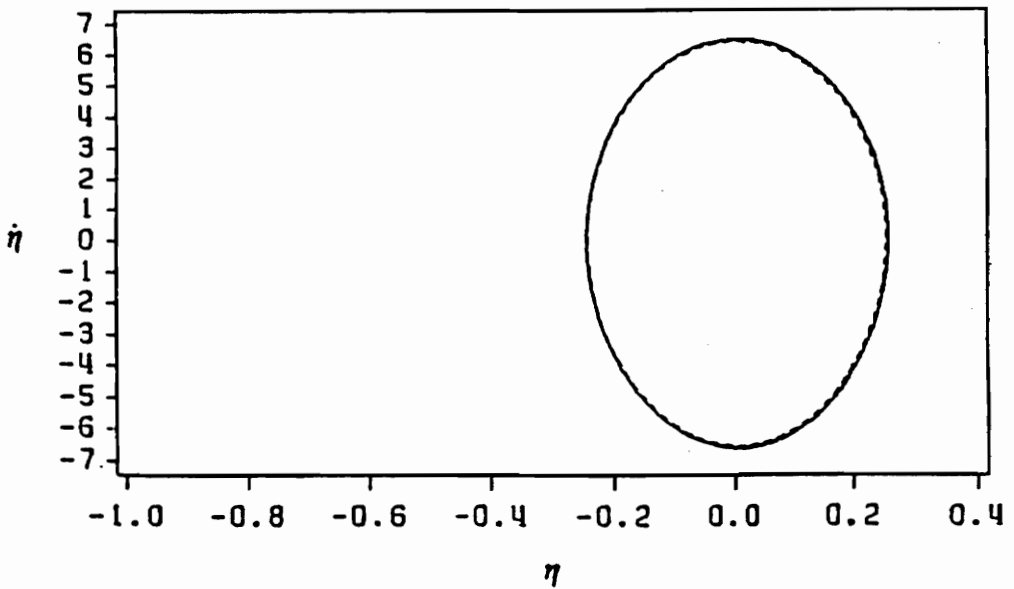


Figure 15. Comparison of perturbation and numerical solutions for case of subharmonic resonance: (a) Time history and (b) phase-plane comparison of perturbation (---) and numerical (___) solutions for $\Omega = 26.0$ rad/sec.

and its phase portrait are shown in Figures 15a and 15b for $\Omega = 26$ rad/sec. Figures 15a and 15b show that there is good agreement between the results of the numerical simulation and the perturbation solution. To form an overall comparison, we plot in Figure 14 the maximum values of η obtained from the perturbation solution (frequency-response curve) and the numerical simulation. Again we have good agreement.

4.4 Stability of Periodic Solutions

To determine the stability of the periodic solutions predicted by the perturbation analysis, we used Floquet theory. We computed η and a from equations (4.28) and (4.33) and then integrated equation (3.23) with the initial conditions given by equations (3.26) and equation (3.27) over the interval $t = [0, T]$. The analytical solution predicted the loss of stability of the primary-resonant solution very accurately as can be seen in Figure 16 (curves P_3 and P_4). To predict the sequence of period-doubling bifurcations that lead to chaos, we integrated the same equations but over an interval of $2T$. The interval $2T$ was used because we are interested in the loss of stability of the subharmonic response. As was the case for primary resonance, the analytical solution had difficulty in predicting the occurrence of period-doubling bifurcations leading to chaos, as can be seen in Figure 16.

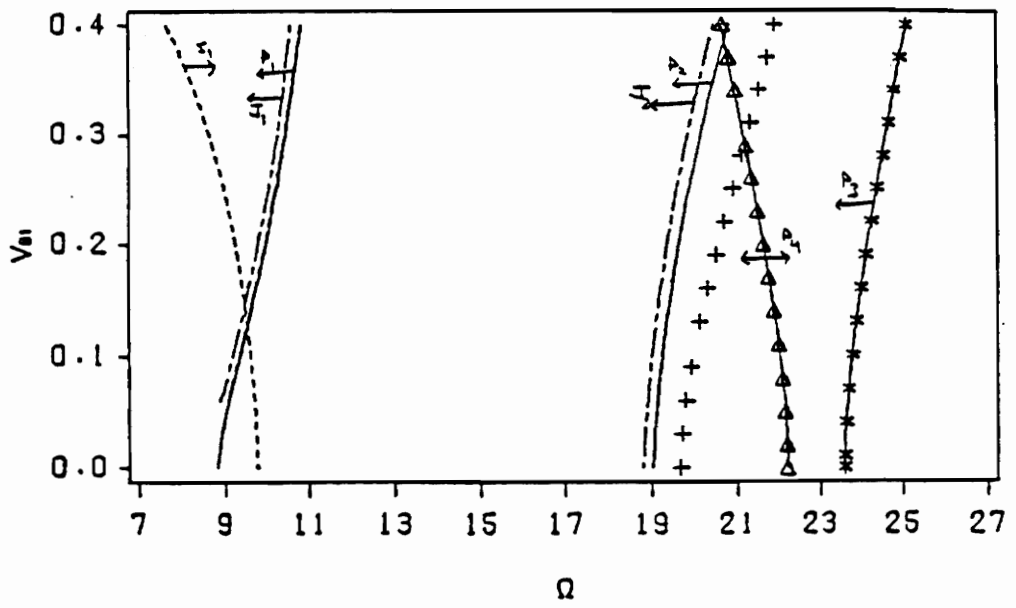


Figure 16. Stability of perturbation solution for case of subharmonic resonance

CHAPTER 5

Conclusions

5.1 *Present Work*

The concept of an infinite-busbar is fictitious yet it is very useful. A more realistic concept of a busbar whose voltage is modulated in magnitude and angle has been introduced by Tamura and co-workers (1984, 1987). Hamdan and Nayfeh (1979) enhanced the concept of a quasi-infinite busbar by including quadratic and cubic nonlinearities. To determine the period-one responses and the onset of period-doubling bifurcations, we use the method of multiple scales to develop an approximate closed-form expression for the response of the machine for the case of primary resonance. The analytical results are in good agreement with the results of the digital-computer simulation. Using Floquet theory and other approximate methods, we determine the conditions

under which the analytically predicted periodic solution loses its stability. These conditions are in good agreement with those obtained by the digital-computer simulation for the onset of the period-doubling bifurcations and the jump to either a large attractor or an unbounded motion (loss of synchronism). To help understand the effect of parameter variations on the system's response, we determined a bifurcation diagram in the two parameter space (Ω vs. V_{B1}). The sensitivity to initial conditions was studied by integrating the equations of motion to locate the regions of attraction for bounded and unbounded motions. We showed that parameter variations had a very considerable affect on the regions of stability.

It was demonstrated by numerical simulation the existence of complex dynamics in a single-machine-quasi-infinite-busbar system due to the simultaneous occurrence of a principal parametric resonance and a subharmonic resonance of order one-half. By decreasing the frequency of excitation we showed that oscillatory solutions (limit-cycles) lose their stability through a series of period-doubling bifurcations leading to chaos and unbounded motions. We formulated a second-order approximate solution that improves on the accuracy of the solution given by Hamdan and Nayfeh (1989). Our solution accounts for the frequency shift caused by the combined effect of the excitations. The loss of stability of the second-order solution, which is a precursor to chaos and unbounded motions, agrees fairly well with the numerical simulations. As for the case of primary resonance, bifurcation

diagrams and basins of attraction were studied. For the subharmonic case, however, we noticed that the interaction of the voltage and phase of the quasi-infinite busbar has a substantial affect on the system's stability.

5.2 *Future Work*

The next step in our analysis is to study the case of two machines connected to an infinite busbar, resulting in a two-degree of freedom system. Many aspects of the complicated dynamics that result are due to internal resonances. Also, of interest are the effect of a quasi-infinite busbar and feedback control on the two machine system.

References

P. M. Anderson and A. A. Fouad, *Power System Control and Stability*, The Iowa State University Press, 1977.

P. Berge, Y. Pomeau, and C. Vidal, *Order Within Chaos*, Wiley-Interscience, New York, 1984.

J. Carr, *Applications of Center Manifold Theory*, Springer-Verlag, New York, 1981.

H. D. Chiang, M. W. Hirsch, F. F. Wu, "Stability Regions of Nonlinear Autonomous Dynamical Systems," *IEEE Transactions on Automatic Control*, Vol. 33, No.1, pp. 16-27, 1988.

Dandeno, "General overview of steady-state (small signal) stability in bulk electricity systems: a North American perspective," *Electrical Power Energy Systems*, Vol. 4, pp. 253-264, 1982.

J.P. Eckmann and D. Ruelle, "Ergodic theory of chaos and strange attractors," *Review of Modern Physics*, Vol. 5, No. 3, pp. 617-656, 1985.

M. J. Feigenbaum, "Quantitative universality for a class of non-linear transformations", *Journal of Statistical Physics*, Vol. 19, p. 25, 1978.

P. Fredrickson, J. L. Kaplan, E. D. Yorke, "The Liapunov Dimension of Strange Attractors," *Journal of Differential Equations*, Vol. 49, pp. 185-207, 1983.

C. Grebogi, E. Ott, S. Pelikan, and J. A. Yorke, "Strange Attractors that are not Chaotic," *Physica D*, Vol. 13, pp. 261-268, 1984.

C. Grebogi, E. Ott, and J. Yorke, "Metamorphoses of Basin Boundaries in Non-Linear Dynamics Systems," *Phy. Rev. Ltr.*, Vol. 56, p. 1011, 1986.

J. Guckenheimer and P. J. Holmes, *Nonlinear Oscillations, Dynamical Systems and Bifurcation Vector Fields*, Springer-Verlag, New York Inc., 1983.

M. W. Hirsch and S. Smale, *Differential Equations, Dynamical Systems and Linear Algebra*, Academic Press, Inc., 1974.

H. M. A. Hamdan, A. M. A. Hamdan, and B. Kahhaleh, "Damping of power system oscillations using a current feedback signal," *Proceedings of the IEE*, Vol. 136, Part C, pp. 137-144, 1989.

A. M. A. Hamdan and A. H. Nayfeh, "The Effect of Nonlinearities on the Response of a Single-Machine Quasi-Infinite Busbar System," *IEEE Transactions on Power Systems*, Vol. PWRS-4, pp. 843-849, 1989.

F. M. Hughes and A. M. A. Hamdan, "Design of turboalternator excitation controllers using multivariable frequency response methods," *Proceedings of the IEE*, Vol. 123, pp. 901-905, 1976.

IEEE Task Force, "Proposed terms and definitions for power system stability," *IEEE Trans. Power Appar. & Syst.*, Vol. PAS-101, 1982, pp. 1894-1898.

G. looss and D. Joseph, *Elementary Stability and Bifurcation Theory* , Springer-Verlag, New York, 1980.

O. E. Lanford, In *Hydrodynamic Instabilities and the transition to Turbulence*, H. L. Swinney and J. P. Gollub (eds.), Springer-Verlag, New York, Chapter 2, 1981.

A. J. Lichtenberg and M. A. Lieberman, *Regular and Stochastic Motion* , Springer-Verlag, New York Inc., 1983.

B. Mandelbrot, *The Fractal Geometry of Nature*, Freeman, San Francisco, 1982.

A. I. Mees, *Dynamics of Feedback Systems*, Wiley Interscience, New York, 1981.

R. K. Miller and A. N. Michel, *Ordinary Differential Equations*, Academic Press, Inc., New York, 1982.

F. C. Moon, *Chaotic Vibrations, An Introduction for Applied Scientists and Engineers*, Wiley-Interscience, 1987.

A. H. Nayfeh, "Perturbation Methods in Nonlinear Dynamics," In *Nonlinear Dynamics Aspects of Particle Accelerators, Lecture Notes in Physics*, No. 247, Springer-Verlag, New York, 1986, pp.238-314.

A. H. Nayfeh, *Perturbation Methods* , Wiley-Interscience, New York, 1973.

A. H. Nayfeh, *Introduction to Perturbation Techniques* , Wiley-Interscience, New York, 1981.

A. H. Nayfeh and D. T. Mook, *Nonlinear Oscillations* , Wiley-Interscience, New York, 1979.

A. H. Nayfeh and N. E. Sanchez, "Bifurcations in a Forced Softening Duffing Oscillator," *Int. J. Non-Linear Mechanics*, Vol. 24, pp. 483-497, 1989.

S. Newhouse, D. Ruelle, and F. Takens, "Occurrence of Strange Axiom A attractors near quasiperiodic flows on $T^m, m \geq 3$," *Communications in Mathematical Physics*, Vol. 64, p. 35, 1978.

Pai, *Power System Stability-Analysis by the Direct Method of Lyapunov*, North Holland, New York, 1981.

T. S. Parker and L. O. Chua, *Practical Numerical Algorithms for Chaotic Systems*, Springer-Verlag, New York Inc., 1989.

Y. Pomeau and P. Manneville, "Intermittent transition to turbulence in dissipative dynamical systems," *Communications in Mathematical Physics*, Vol. 74, p.189, 1980.

R. A. Raouf, "Modal Interactions in Shell Dynamics," Department of Engineering Science and Mechanics, Virginia Polytechnic Institute and State University, Blacksburg, Virginia. 1989.

D. Ruelle and F. Takens, "On the nature of turbulence," *Communications in Mathematical Physics*, Vol. 20, p. 167, 1971.

N. E. Sanchez, "Stability of Nonlinear Oscillatory Systems with Application to Ship Dynamics," Department of Engineering Science and Mechanics, Virginia Polytechnic Institute and State University, Blacksburg, Virginia, 1989.

R. Seydel, *From Equilibrium to Chaos: Practical Bifurcation and Stability Analysis*, Elsevier Science Publishing Co., Inc., New York, 1988.

M. S. Soliman and J. M. T. Thompson, "Integrity Measures Quantifying the Erosion of Smooth and Fractal Basins of Attraction," *J. Sound Vib.*, Vol. 135, pp. 453-475, 1989.

Y. Tamura, N. Yorino, H. Mori, and S. Iwamoto, "On the Possibility of Parametric Resonance in Power Systems - A New Concept of Power System Stability," *Proceedings PSCC*, pp. 939-946, 1984.

T. Tamura and Y. Yorino, "Possibility of Auto- and Hetero- Parametric Resonances in Power Systems and their Relationship with Long-Term Dynamics," *IEEE Transactions on Power Systems*, Vol. PWRS-2, pp. 890-897, 1987.

J. M. T. Thompson and H. B. Stewart, *Nonlinear Dynamics and Chaos, Geometric Methods for Engineers and Scientists*, John Wiley and Sons Ltd., 1986.

P. Varaiya, F. F. Wu, and R. Chen, "Direct Methods for Transient Stability Analysis: Recent Results," *Proceedings of the IEEE*, Vol. 73, No. 12, pp. 1703-1705, 1985.

A. Wolf, J. B. Swift, H. L. Swinney, and J. A. Vastano, "Determining Lyapunov Exponents from a Time Series," *Physica D*, Vol. 16, pp. 285-317.

J. Zaborsky, G. Huang, B. Zheng, and T. Leung, "On the Phase Portrait of a Class of Large Nonlinear Dynamic Systems such as Power Systems," *IEEE Transactions on Automatic Control*, Vol. 33, No. 1, pp. 4-15, 1988.

Appendix A

Coefficients in Expanded Form of Swing Equation

$$\alpha_2 = \frac{1}{2} K \tan \delta_0, \alpha_3 = \frac{1}{6} K,$$

$$F_1 = -\frac{V_{B1}}{V_{B0}} K, F_2 = \frac{V_{B1}}{2V_{B0}} K \tan \delta_0,$$

$$F_3 = \frac{V_{B1}}{6V_{B0}} K, G_1 = \Omega^2 \theta_{B1},$$

$$G_2 = \frac{\Omega D \omega_R \theta_{B1}}{2H}, G_3 = -\frac{V_{B1}}{V_{B0}} K \tan \delta_0,$$

$$K = \frac{V_G V_{B0} \omega_R \cos \delta_0}{2HX_6}$$

Appendix B

Parameters of Machine Used in Chapter 3

The parameters of the machine have been taken from Table D3 of Appendix D of the textbook of Anderson and Fouad (1977). They are

Rated MVA = 160, Rated PF = 0.85, Rated KV = 15,

Freq = 60 Hz, $X'_d = 0.245$, H = 2.37 S,

The rest of the parameters of the SMQIBS are

$X_{line} = 0.4$ per unit, $V_{B0} = 1$ per unit, $V_{B1} = 0.1$ per unit,

$\theta_{B1} = 0.1$ rad,

$X_G = X_{line} + X'_d = 0.645$ per unit

D is varied between 0.002 - 0.016.

Appendix C

Coefficients for Stability Analysis

$$K^* = K + \left(\frac{3\alpha_3}{2} - \frac{\alpha_2^2}{3\Omega^2} \right) a^2 - \frac{19\alpha_2^2\alpha_e a^4}{24\Omega^4}$$

$$\chi = 2\alpha_2 a + \frac{5\alpha_2\alpha_3 a}{2\Omega^2}$$

$$\Lambda = \left(\frac{3\alpha_3}{2} - \frac{\alpha_2^2}{3\Omega^2} \right) a^2 - \frac{\alpha_2^2\alpha_3 a^4}{2\Omega^4}$$

$$\gamma_1 = -720(K^* - 2\mu^2)$$

$$\gamma_2 = -4(99\chi^2 - 472K^{*2} + 576\mu^2 K^* - 576\mu^4 + 18\Lambda^2)$$

$$\gamma_3 = 39[(19K^* - 6\mu^2 + 9\Lambda)\chi^2 - 40K^{*3} + 80\mu^2 K^{*2} + (10 - 12\mu^2)\Lambda]$$

$$\gamma_4 = 16[\chi^2 - 2(K^* + \Lambda)\chi - 4K^{*2} + \Lambda^2][\chi^2 + 2(K^* + \Lambda)\chi - 4K^{*2} + \Lambda^2]$$

Appendix D

Parameters of Machine Used in Chapter 4

The parameters of the machine have been taken from Table D3 of Appendix D of the textbook of Anderson and Fouad¹. They are

Rated MVA = 160, Rated PF = 0.85, Rated KV = 15,
Freq = 60 Hz, $X'_d = 0.245$, H = 2.37 S,

The rest of the parameters of the SMQIBS are

$X_{line} = 0.4$ per unit, $V_{B0} = 1$ per unit, $V_{B1} = 0.2$ per unit,
 $\theta_{B1} = 0.2$ rad, D = 0.004
 $X_G = X_{line} + X'_d = 0.645$ per unit

Vita

The author was born in San Bernardino, California on May 24, 1967. He earned the Bachelor of Science degree in Electrical Engineering at Virginia Polytechnic Institute and State University (VPI&SU) in 1988. He continued his education at VPI&SU and earned his Masters degree in Electrical Engineering in 1990.